

ORIGINAL ARTICLE

Optimization-based multitarget stacked machine-learning model for estimating mechanical properties of conventional and fiber-reinforced preplaced aggregate concrete

M. A. Saleh^{1,2} · F. Kazemi^{3,4}  · H. S. Abdelgader⁵ · H. F. Isleem⁶

Received: 1 November 2024 / Revised: 6 May 2025 / Accepted: 13 May 2025

© The Author(s) 2025

Abstract

Nowadays, using advanced structural materials such as preplaced aggregate concrete (PAC) and fiber-reinforced preplaced aggregate concrete (FR-PAC) are widely investigated due to their benefits in designing infrastructures. Therefore, finding the mechanical characteristics of PAC and FR-PAC can help structural engineers. This study explores the material characteristics, performance, and potential challenges associated with using PAC and FR-PAC, aiming to provide insights into their practical implementation and long-term benefits in construction. In addition, a superior estimation tool based on multi-target stacked machine-learning (ML) model was introduced to reduce the cost of experimental tests and increase the accuracy and speed of finding the best mixture for PAC and FR-PAC. Experimental tests were conducted to prepare unseen dataset to validate the general ability of the ML models. Results show that the proposed multi-target stacked ML models can estimate the compressive and tensile strengths of PAC specimens with an accuracy of 97.4% and 94.7%, respectively; however, for compressive, flexural, and tensile strengths FR-PAC specimens, the accuracy of 97.7%, 98.0% and 98.3%, were determined, respectively. The proposed predictive model was turned into a graphical user interface (GUI) with ability on predicting the mechanical properties of PAC and FR-PAC in different curing day, and updating the database in future.

Keywords Preplaced aggregate concrete · Fiber-reinforced preplaced aggregate concrete · Stacked machine-learning model · Data processing · Multitarget machine-learning model

1 Introduction

Preplaced aggregate concrete (PAC) is a unique form that coarse aggregates are pre-placed in molds, and then a cementitious grout injected by pressure. This method has been extensively studied for its potential in applications requiring high-density and high-strength concrete, such as marine structures and heavyweight concrete [1]. Experiments have demonstrated that PAC can achieve superior mechanical properties compared to conventional concrete, particularly when enhanced with supplementary cementitious materials (SCMs) and fibers [2]. Studies involving the incorporation of fly ash, silica fume, and other SCMs into PAC have shown significant improvements in both workability and strength. Fly ash, for instance, has been used to replace up to 50% of cement in PAC mixtures [3], resulting in improved flowability, extended handling times, and reduced water requirements as confirmed in [4]. This substitution not only enhances the fresh properties of PAC but also contributes to



sustainability by reducing cement consumption [5]. Silica fume, despite increasing the water demand due to its fine particle size, substantially boosts the mechanical strength of PAC [6]. Similarly, metakaolin has been noted to improve the grout's mechanical properties and resistance to bleeding, albeit with a decrease in flowability [2]. The role of aggregates in PAC is pivotal, as they constitute around 60% of its volume. The use of high-quality coarse aggregates and appropriate sand grading is crucial for achieving optimal strength and durability. Superplasticizers are often added to PAC to enhance the flowability of the grout, ensuring complete void filling without segregation [7]. The placement method, either by gravity or injection, also influences the final properties of PAC, with injected grouts typically providing better performance in terms of uniformity and strength [8].

Because compaction is not necessary when aggregates are pre-placed, production costs are decreased. Abdelgader et al. [9] constrained the amount of coarse aggregate in the mixture to a minimum while considering the segregation, pumpability, and workability of grout ensuring complete grout penetration is essential for producing high-quality PAC. Therefore, grout needs to be sufficiently flowable to fill voids without separating. PAC's unique placement strategy offers several advantages in terms of technology and sustainability. The use of aggregate types that would otherwise pose challenges in the concrete production process is made possible by placing aggregates in the formwork prior to grout injection. As an example, using very heavy aggregates, such as magnetite, when producing concrete can help avoid segregation issues, which is desirable when building nuclear power plants. Furthermore, the PAC method will not experience concrete casting issues when using recycled concrete aggregates, which often have a higher water absorption rate, which leads to a loss of workability and serious pumping problems [10]. In addition, the coarse aggregate that makes up most of the volume of the concrete in PAC is mixed without the use of a concrete mixer. This considerably shortens the time needed to mix the concrete, which expedites construction. Additionally, it requires less energy to mix and pump concrete. The integration of fibers, particularly steel fibers, into PAC has shown significant benefits in improving its mechanical properties [11]. Research has demonstrated that the inclusion of steel fibers enhances the tensile and flexural strength of PAC, reduces crack formation, and increases ductility through a crack-bridging mechanism [12]. Studies have particularly highlighted the efficacy of using various fiber lengths and dosages [13], with higher dosages yielding substantial improvements in compressive, tensile strength [14], and flexural strength [15].

Recent studies highlight the efficacy of ML techniques in predicting concrete compressive strength (as the main contribution in [16]), showcasing a departure from traditional regression methods [17]. Among various ML algorithms, artificial neural networks (ANNs) have been prominently used with impressive accuracy [18]. Chithra et al. [19] employed ANN to forecast the compressive strength of copper slag and silica nanoparticle-infused high-performance concrete (HPC), while Ayat et al. [20] achieved a high correlation coefficient (0.976) for limestone-filled concrete. The support vector machine (SVM) model also demonstrated superior predictive capabilities for lightweight concrete, as evidenced by Kumar et al. [21]. Similarly, Nguyen et al. [22] identified gradient boosting machine (GBM) and extreme gradient boosting (XGBoost) as highly accurate for HPC strength predictions. Zhang et al. [23] utilized random forest (RF) for lightweight self-compacting concrete, performing detailed input variable analysis. Statistical methods, though beneficial, are limited by admixture constraints [24], leading researchers to further explore ML for prediction of concrete strength [25], high-performance concrete [26], and recycled concrete materials [27]. Other notable algorithms include decision tree (DT) [28], gene expression programming (GEP) [29], and multi-expression programming (MEP) [30]. These techniques typically involve training, validation, and testing phases to ensure robust model performance and prevent overfitting [31]. Machine learning (ML) has become an invaluable tool in predicting the properties of PAC, significantly enhancing the accuracy and efficiency of these predictions while minimizing the need for extensive physical testing. Notably, Moaf et al. [32] demonstrated the potential of ML algorithms such as extra trees regressor (ETR), random decision forest (RF), and bagging regression (BR) in predicting PAC compressive and tensile strength with high accuracy, achieving compressive strength prediction accuracies of 98.3%, 95.3%, and 94.6%, respectively. These models effectively reduce the experimental burden while maintaining accuracy. Qureshi et al. [33] extended this line of research by comparing the performance of gene expression programming (GEP) and RF models in predicting PAC compressive strength using a dataset of 135 compressive strength (CS) values and 11 input variables. Their

findings revealed that the RF model, with an R^2 value of 0.96, outperformed GEP, which had an R^2 of 0.94, and demonstrated lower statistical errors. The study's SHAP analysis further identified superplasticizer content and water-to-binder ratio (W/B) as critical factors influencing PAC strength, underscoring the environmental and economic benefits of optimizing material use through ML. Further advancements in ML applications for PAC strength prediction were reported by Javed et al. [34] who evaluated thirteen ML models using a dataset of 261 data points. Their analysis identified XGBoost as the most accurate model, with a correlation coefficient of 0.9791 and an R^2 of 0.9583. Additionally, models like GBM, CatBoost, and RF also yielded precise predictions with minimal errors. Abdellatif et al. [35] focused on predictive algorithms to achieve desired properties such as CS of foam concrete by optimizing mix designs and addressing traditional design limitations. They employed 261 experimental results and showed that the Gaussian process regression (GPR) algorithm achieved the highest accuracy (R^2 value of 0.98). Furthermore, parametric and sensitivity analyses were conducted for estimating effect of input variables on foam concrete. Moreover, Abdellatif et al. [36] developed ML models to predict CS of ultra-high-performance geopolymer concrete using 113 available test results and 128 additional conducted experiments. The analysis confirmed the robust predictive capability of the RF, SVR, and XGBoost models, each achieving excellent performance with R^2 more than 0.84, while XGBoost model demonstrated superior accuracy.

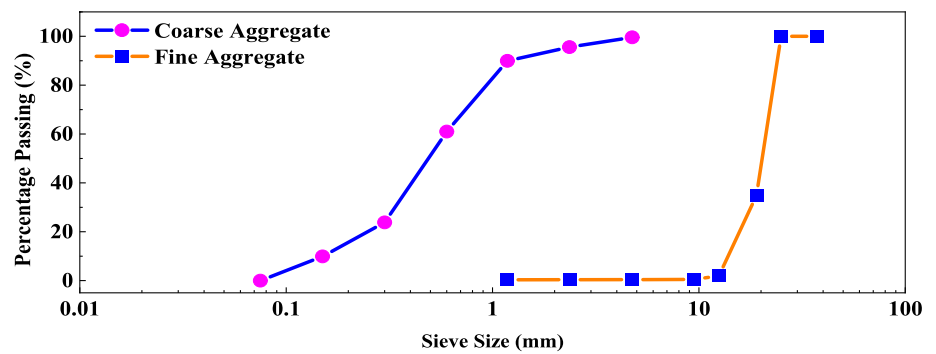
Although some studies have been conducted to provide predictive models for the prediction of mechanical strengths of PAC, the proposed models were stands on the provided dataset and could not be implemented on the new dataset. To tackle these shortcomings, this study introduced optimization-based multi-target stacked ML models to predict the compressive, flexural and tensile strengths of PAC and FR-PAC. Due to a smaller number of available datasets, synthetic data generation methods such as variational autoencoders (VAEs) and generative adversarial networks (GANs) have been used to learn the underlying distribution of real data and generate new, similar data points. In addition, K-nearest neighbors (KNN) imputation has been used as a technique to handle missing values in datasets, which can enhance the ability of the proposed ML models. Different data resampling methods such as edited nearest neighbors (ENN) and k-fold cross validation (CV) have been used to prepare dataset for ensemble methods. However, the proposed ML models are hyperparameter free and can be tuned by innovative approaches of grey wolf optimizer (GWO), particle swarm optimization (PSO), and non-dominated sorting PSO (NSPSO) that is a modified version of PSO for multi-objective optimization. Since the validation of the proposed predictive model can assure of its capability, experimental specimens of PAC and FR-PAC were constructed and tested to prepare unseen dataset. Capability and reliability of the proposed optimization-based multi-target stacked ML models were checked by the provided experimental dataset for future applications. Then, a graphical user interface (GUI) is proposed as a preliminary estimation tool for the compressive and tensile strength of PAC and FR-PAC and can be used for design purposes.

2 Experimental study on preplaced aggregate concrete

The following sections delineate the material preparation, mixture design, and experimental testing protocols employed in this study.

2.1 Material preparation

The materials used in the preparation of PAC are carefully selected and prepared to ensure consistency and reproducibility in the production of concrete with desirable mechanical properties. The primary binding material used in all grout mixtures was Portland limestone cement (PLC) with specific gravity and surface area equal to 3.05 and 1199 m^2/kg , respectively. SCMs were integrated to replace PLC, including fly ash (FA), silica fume (SF), metakaolin (MK). Each SCM possesses unique physical and chemical properties that influence the performance characteristics of the PAC. For instance, FA is known for enhancing workability and reducing the heat of hydration, while SF significantly improves strength and durability due to its high silica content.

Fig. 1 Sieve presentation of aggregates**Fig. 2** Types of fibers used in this study: **a** short hooked-end steel fibers, **b** long hooked-end steel fibers, **c** polypropylene fibers, and **d** glass fibers

The fine aggregate utilized comprised silica sand with a saturated surface dry specific gravity of 2.6, a water absorption rate of 1.63%, and a fineness modulus of 2.2. The coarse aggregates used were crushed granite, ranging in size from 10 mm to 25 mm, possessing specific gravity and water absorption equal to 2.69 and 1.07%, respectively. Both aggregates were thoroughly washed to remove impurities and enhance the bonding with the grout. The gradation curve for aggregates is presented in Fig. 1. In addition, four types of fibers were used, short and long monofilament hooked-end steel fibers, alkali-resistant glass fibers (GF) and polypropylene fibers (PP). The fiber content in this study varied with specific volume fractions, Fig. 2 depicts the visual characteristics of the fibers used. A poly-carboxylate superplasticizer, named PC-303, was utilized to improve the workability of the grout mixtures. The superplasticizer, with a solid content of 96% and a density of 0.7 g/cm^3 , was optimized through various trials to achieve an efflux time of $35\text{--}40 \pm 2 \text{ s}$, as stipulated by ASTM C939 [37].

Table 1 PAC mixture proportions

Grout mixture No.	Grout mixture notation	Binder (kg/m ³)				Sand (kg/m ³)	Gravel (kg/m ³)	Water (kg/m ³)
		PLC	FA	SF	MK			
C	100PLC	344	0	0	0	344	1610	155
F1	90PLC-10FA	307	34	0	0	341	1610	153
F2	80PLC-20FA	271	68	0	0	339	1610	153
F3	70PLC-30FA	235	101	0	0	336	1610	151
S1	90PLC-10SF	306	0	34	0	340	1610	153
SF1	80PLC-10FA-10SF	270	34	34	0	338	1610	152
SF2	70PLC-20FA-10SF	234	67	34	0	335	1610	151
M1	90PLC-10MK	308	0	0	34	342	1610	154
MF1	80PLC-10FA-10MK	272	34	0	34	340	1610	153
MF2	7PLC-20FA-10MK	236	67	0	34	337	1610	152

Table 2 Mixture proportions of FR-PAC mixtures

Mixture	Fiber type	Fiber percentage (%)	S/B	W/B	Superplasticizer (%)
C	–	0	1.0	0.45	0.02
SL01	Long steel	1	1.0	0.45	0.02
SL02		2	1.0	0.45	0.02
SL04		4	1.0	0.45	0.02
SL06		6	1.0	0.45	0.02
SS01	Short steel	1	1.0	0.45	0.02
SS02		2	1.0	0.45	0.02
SS04		4	1.0	0.45	0.02
SS06		6	1.0	0.45	0.02
PP01	Polypropylene	1	1.0	0.45	0.02
PP02		2	1.0	0.45	0.02
PP04		4	1.0	0.45	0.02
PP06		6	1.0	0.45	0.02
GF01	Glass fibers	1	1.0	0.45	0.02
GF02		2	1.0	0.45	0.02

2.2 Mixture design

The mixture design for PAC necessitates precise proportioning of materials to achieve optimal mechanical properties. The primary binding material was PLC, and SCMs such as FA, SF, and MK were used in varying proportions to partially replace PLC. The sand-to-binder ratio (S/B) was maintained at 1.0, and W/B was set at 0.45. The grout mixtures with SCM replacement proportions were selected to align with previous research [2, 38], which investigated similar percentages of SCMs and identified fly ash as the main binder replacement for ordinary Portland cement in PAC. This approach ensures consistency with established practices and enables a direct comparison of PAC’s performance with widely studied SCMs under similar conditions. Table 1 presents the proportions of PAC mixtures, while Table 2 presents the proportions of FR-PAC mixtures used in this study.

The mixing procedures adhered to ASTM C938 standards [39], involving preplacing aggregates into formworks then dry mixing sand and cementitious materials for two minutes, followed by progressively adding the superplasticizer and mixing water over five minutes until achieving homogeneity then injecting the grout into the formworks. The addition of fibers required adjustments in the mixture design to ensure proper dispersion

Table 3 PAC grouts fresh properties

Grout mixture ID	Optimum superplasticizer dosage (%)
C	0.02
F1	0.02
F2	0.01
F3	0.03
S1	0.08
SF1	0.06
SF2	0.06
M1	0.09
MF1	0.05
MF2	0.05



Fig. 3 PAC's mixing procedure, **a** positioning coarse aggregates by injection tubes in cylinder molds above shaker machine; **b** PAC mixtures after grout injection; **c** molded specimens; and **d** curing of specimens in curing room

and effectiveness. The fibers were uniformly distributed with the coarse aggregates to avoid clumping and ensure homogeneity before injecting the grout.

2.3 Experimental test

Experimental testing of PAC and FR-PAC involved a comprehensive evaluation of mixtures properties. Fresh grout flowability was determined by the flow cone method [35], targeting an efflux time of $35\text{--}40 \pm 2$ s using a superplasticizer. Table 3 displays the results of the optimum superplasticizer dosage for each mixture to produce the target efflux time. Compressive and tensile strength tests were conducted on $150\text{ mm} \times 300\text{ mm}$ cylindrical samples at 7, 28, and 90 days, following ASTM C943 [40]. In addition, the flexural performance of FR-PAC prisms ($150\text{ mm} \times 150\text{ mm} \times 550\text{ mm}$) was evaluated after 28 days by a three-point bending test, following the specifications outlined in ASTM C1609 [41]. Figures 3 and 4 show the mincing procedures of PAC and FR-PAC specimens. Firstly, preplacing coarse aggregates and fibers into oiled molds, followed by the gravity-based grout injection process, and then cured at $20\text{ }^\circ\text{C}$ with 99% relative humidity for the designated testing periods. The compressive strength tests were performed using a universal testing machine (Fig. 5), with an applied loading of 0.25 MPa/s until failure. These tests provided valuable insights into the mechanical performance of PAC, facilitating the development of mixtures with superior attributes.

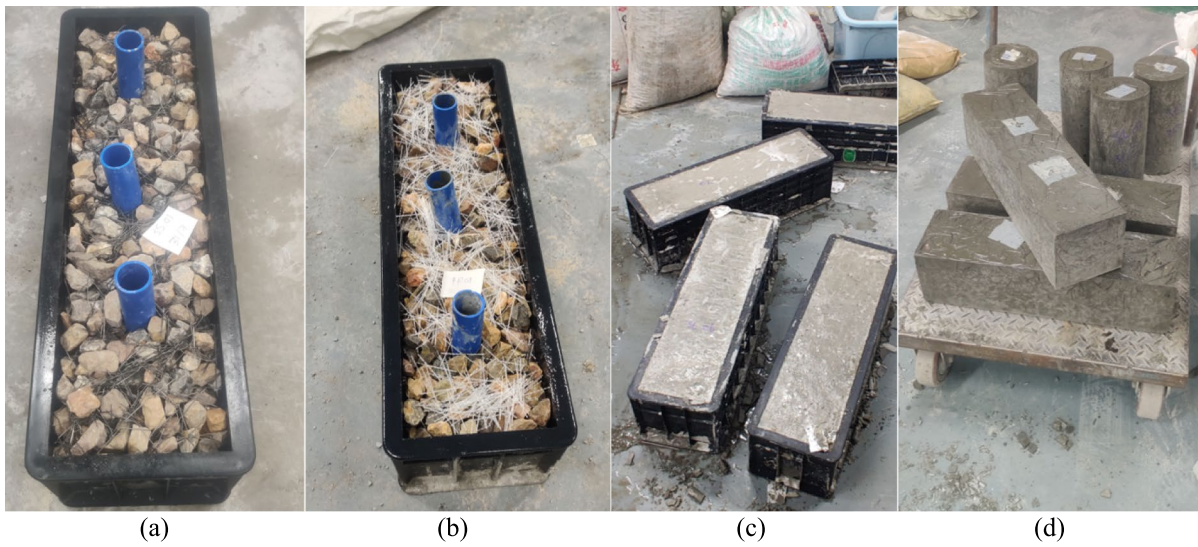


Fig. 4 FR-PAC mixing procedure, **a** preplacing aggregates, fibers and injection tubes into prism molds; **b** preplacing injection tubes, aggregates and fibers prior to injecting grout in prism molds; **c** specimens following grout injection; and **d** demolded specimens



Fig. 5 Compressive strength test setup on PAC and FR-PAC samples

2.4 Results and discussion of experimental tests

2.4.1 Compressive strength of PAC

The results, encompassing various binder combinations and SCMs, are illustrated in Fig. 6. The compressive strength outcomes demonstrate distinct trends based on the type and proportion of SCMs used. The data indicates a clear relationship between the type of binder and compressive strength. Increasing FA replacement level for PLC concluded a notable reduction in compressive strength. Specifically, an increase in FA from 10% to 30% in the grout reduced the compressive strength of PAC after 7 days by approximately 32.4%, compared to the control mixture. Similarly, the substitution of 30% of PLC with FA led to a significant decrease in compressive strength, with a reduction of up to 28%. The compressive strength of mixture F3 decreased from 27.2 MPa to 19.5 MPa over 90 days, illustrating the impact of FA's slower hydration process during the early curing stages. In contrast, mixtures incorporating SF or MK showed substantial improvements in compressive strength due to their high pozzolanic activity and ability to enhance particle packing density. The S1 mixture, containing 10% SF, achieved the highest compressive strength at 90 days (36.9 MPa), representing a significant increase of 35.6% compared to the control mixture.

Detailed compressive strength of PAC in different curing days is presented in Table 4. The second-highest compressive strength was observed in the SF1 mixture, which contained 10% SF and 10% FA. Compared to the example mixture, the SF1 mixture exhibited compressive strength increases of 38.5%, 90.5%, and 34.0% at 7, 28, and 90 days, respectively. This highlights the SF effects. The incorporation of MK, either alone or in combination with other SCMs, also demonstrated significant improvements in compressive strength. Mixtures MF1 and MF2, which combined MK and FA, showed reduced compressive strengths compared to mixtures containing only SF. However, these mixtures still outperformed those with FA alone. The results underscore the importance of pozzolanic materials in enhancing the mechanical properties of PAC by filling micropores and promoting the pozzolanic reaction, which in turn improves the microstructure and interfacial

Fig. 6 Compressive strength results of PAC mixture

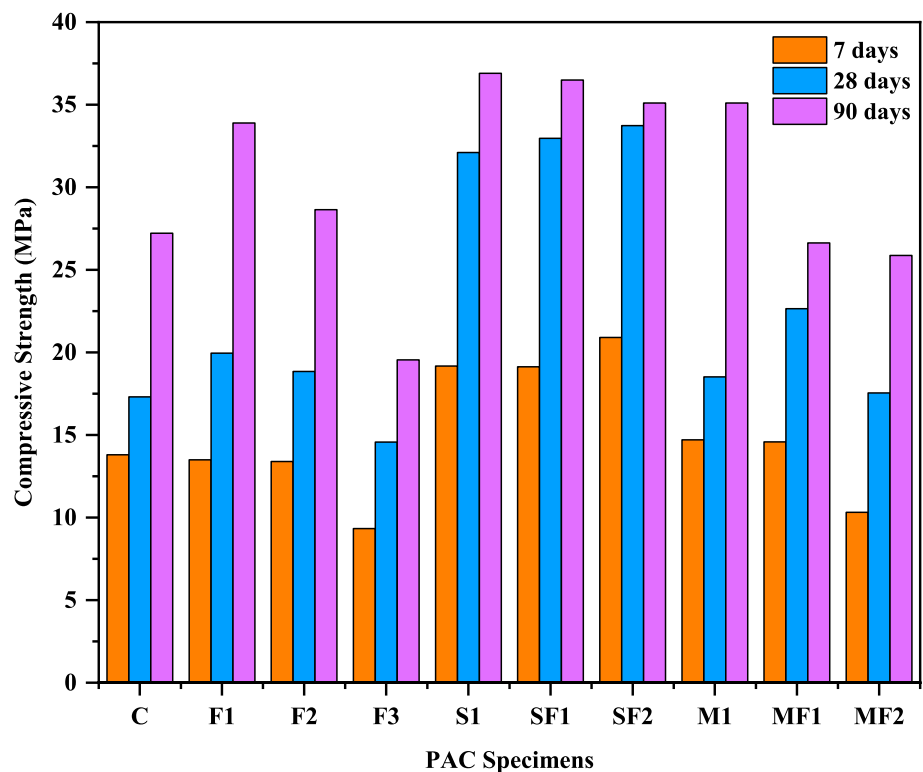


Table 4 Compressive strength of PAC mixtures in all curing

PAC mixture ID	Compressive strength (MPa)			Covariance (%)		
	7 days	28 days	90 days	7 days	28 days	90 days
C	13.8	17.3	27.2	0.08	0.50	0.94
F1	13.5	20.0	33.9	0.06	1.29	0.81
F2	13.4	18.8	28.6	0.33	0.51	2.56
F3	9.3	14.6	19.5	0.62	0.27	0.59
S1	19.2	32.1	36.9	1.03	0.85	2.06
SF1	19.1	33.0	36.5	1.59	1.82	1.09
SF2	20.9	33.7	35.1	1.87	0.07	4.03
M1	14.7	18.5	35.1	0.43	0.37	0.72
MF1	14.6	22.6	26.6	0.30	1.57	4.21
MF2	10.3	17.5	25.9	0.30	0.98	1.60

zone between the grout matrix and the aggregate. The findings indicate that the optimal PAC mixture to gain the highest compressive strength incorporates 10% SF, either alone or in combination with other SCMs. The strategic use of SCMs, particularly SF, significantly enhances the compressive strength of PAC, making it a viable alternative to conventional concrete mixtures.

2.4.2 Compressive strength of FR-PAC

Compressive strength results for the FR-PAC mixtures reveal distinct differences based on the type and percentage of fibers used as presented in Table 5. Among the tested specimens, the inclusion of steel fibers, particularly long steel fibers (SL mixtures), significantly improve the compressive strength of mixtures. For instance, the SL01 mixture with 10% long steel fibers gained a compressive strength of 30.2 MPa, while the SL02 mixture with 20% long steel fibers demonstrated a further increase to 36.2 MPa. The highest compressive strength recorded was 49.8 MPa for the SL06 mixture, indicating a substantial improvement and highlighting the efficacy of long steel fibers in reinforcing concrete. This mixture’s performance surpassed the SL04 mixture, which recorded a compressive strength of 45.1 MPa, suggesting a positive correlation between long steel fibers’ quantity and resultant compressive strength.

Table 5 Compressive strength of FR-PAC mixtures in curing of 28 days

FR-PAC mixture ID	Compressive strength (MPa)	Covariance (%)
C	17.3	2.9
SL01	30.2	1.9
SL02	36.2	3.9
SL04	45.1	3.7
SL06	49.8	0.8
SS01	20.6	2.3
SS02	29.0	1.9
SS04	39.1	1.4
SS06	43.9	6.0
PP01	15.2	3.2
PP02	20.3	8.0
PP04	19.9	4.8
PP06	19.4	2.2
GF01	14.3	7.9
GF02	11.5	10.0

Comparatively, the short steel fibers (SS mixtures) also contributed to notable enhancements in compressive strength, albeit to a slightly lesser extent than their long fiber counterparts did. The SS01 and SS02 mixtures, containing 10% and 20% short steel fibers respectively, showed compressive strengths of 20.6 MPa and 29.0 MPa. Higher percentages of short steel fibers, as seen in SS04 (39.1 MPa) and SS06 (43.9 MPa), further validated the beneficial impact of increased fiber content. Conversely, the PP mixtures and GF mixtures exhibited significantly lower compressive strengths, with the highest values recorded at 20.3 MPa for PP02 and 14.3 MPa for GF01, respectively. Results show the highest performance of steel fibers, particularly long steel fibers, in enhancing the compressive strength of FR-PAC mixtures, making them a preferable choice for applications requiring high-strength concrete.

3 Machine learning model

3.1 Data preparation

The dataset employed in this study consists of 475 datasets, with 419 datasets allocated for PAC and 56 datasets designated for FR-PAC. These datasets have been meticulously gathered from both existing literature and our own experimental work, with 30 datasets for PAC and 14 for FR-PAC originating from our research efforts. The PAC dataset encompasses 14 input variables, which are known to significantly influence its mechanical properties cement (C), FA, SF, ground granulated blast-furnace slag (GGBS), MK, limestone powder (LP), sand (S), water (W), gravel (G), W/B ratio, S/B ratio, superplasticizer (SP), expanding admixture (EA), and curing days (DC). Similarly, the FR-PAC dataset includes 14 input variables, cement, sand, gravel, water, superplasticizers, W/B ratio, S/B ratio, PP, steel fibers (SF), fiber length (FL), fiber diameter (D), aspect ratio (AR), fiber tensile strength (FTS), and days of curing. The predicted output variables for PAC are compressive strength (CS) and tensile strength (TS), while for FR-PAC, CS, TS, and flexural strength (FS) were considered. It should be noted

Table 6 Summary of the experimental PAC datasets used for ML

Output properties	No. of datasets	References
CS* and TS**	35	Abdelgader [42]
CS and TS	63	Abdelgader and Gorski [43]
CS and TS	33	Abdelgader and Elgalhud [7]
CS and TS	15	Coo and Pheeraphan [24]
CS and TS	36	Najjar et al. [2]
CS and TS	10	Coo and Pheeraphan [44]
CS	8	Das and Lam [8]
CS and TS	108	Abdelgader et al. [45]
CS and TS	12	Chairunnisa et al. [46]
CS and TS	58	Das [47]
CS	1	Murali et al. [48]
CS	1	Murali et al. [49]
CS	2	Murali et al. [50]
CS	1	Mohan et al. [51]
CS	2	Ponnambalam et al. [52]
CS	1	Prasad and Murali [53]
CS	1	Karthikeyan et al. [54]
CS	1	Ram Prasad et al. [55]
CS and TS	1	Jaishankar et al. [56]
CS and TS	30	Our work
Total	419	

*Compressive strength, **Tensile strength

Table 7 Summary of the experimental FR-PAC datasets used for ML

Output properties	No. of datasets	References
CS	2	Murali et al. [48]
CS and TS	3	Murali et al. [49]
CS, TS, and FS*	6	Murali et al. [50]
CS	6	Murali et al. [57]
CS	1	Mohan et al. [51]
CS	1	Ponnambalam et al. [52]
CS	1	Swaminathan et al. [58]
CS	2	Prasat et al. [53]
CS	3	Ramakrishnan et al. [59]
CS, TS, and FS	8	Najjar et al. [60]
CS, TS, and FS	2	Jaishankar et al. [56]
CS and TS	5	Alyousef [61]
CS	2	[55]
CS and TS	14	Our work
Total	56	

*Flexural strength

that the training and testing data points have been considered from 80% and 20% of datasets, respectively. Summary of the collected experimental datasets of PAC and FR-PAC are shown in Tables 6 and 7, respectively. To facilitate the creation of robust predictive models, a thorough descriptive analysis of the input variables was conducted, focusing on statistical quantitative indicators. This analysis included calculating minimum, maximum, mean, standard deviation, median, mode, range, skewness, kurtosis, sample variance, sum, and count for each parameter. Such measures of central tendency and dispersion, along with an examination of the shape of data distribution, offer valuable insights into the dataset’s characteristics, highlighting any anomalies or patterns that could influence the performance of machine learning models.

3.2 Data resampling and pre-processing

Data resampling methods are necessary for regression analysis, particularly when dealing with imbalanced datasets, outliers, or the need for data increasing. One fundamental method is bootstrapping, which involves repeatedly drawing samples from the dataset with replacement. This technique aids in estimating the distribution of a statistic, such as the mean, by creating multiple bootstrapped samples, thereby allowing for the assessment of a model’s variability and confidence intervals. Different data resampling methods such as edited nearest neighbors (ENN) and *k*-fold cross validation (CV) have been used to prepare dataset for ensemble methods [62]. ENN cleans the dataset by removing outliers and noise, which can significantly enhance the quality of the training data and, consequently, the model’s performance. This method is particularly useful for regression tasks where the goal is to enhance the predictive performance of a model by refining the dataset. CV, another vital resampling method, partitions dataset into *k* folds and iteratively trains the ML model for *k* times, having different subsets for validation. This approach ensures robust model evaluation and helps model generalizing to unseen data. Using these methods can improve the dataset and thereby performance of ML models.

After preparing datasets, there is a lack of information on some parts of input features and cannot be filled in the datasets. This information can be processed by some novel ML methods that help to predict those input features. Therefore, in this research, KNN imputation has been used as technique to handle missing values in datasets [63]. Once the nearest neighbors are identified, the missing value is imputed by taking the average or the most common value of these neighbors. Therefore, KNN imputation is effective in preserving the underlying data distribution and relationships, making it a robust method for addressing missing values and enhancing the

Fig. 7 Architecture of VAEs and the procedure used for data generation

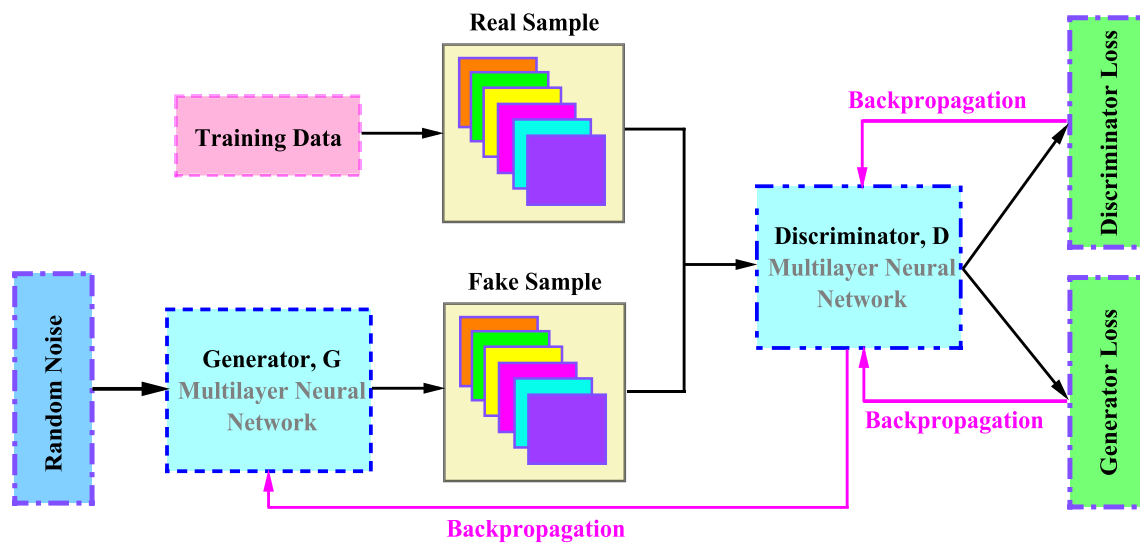
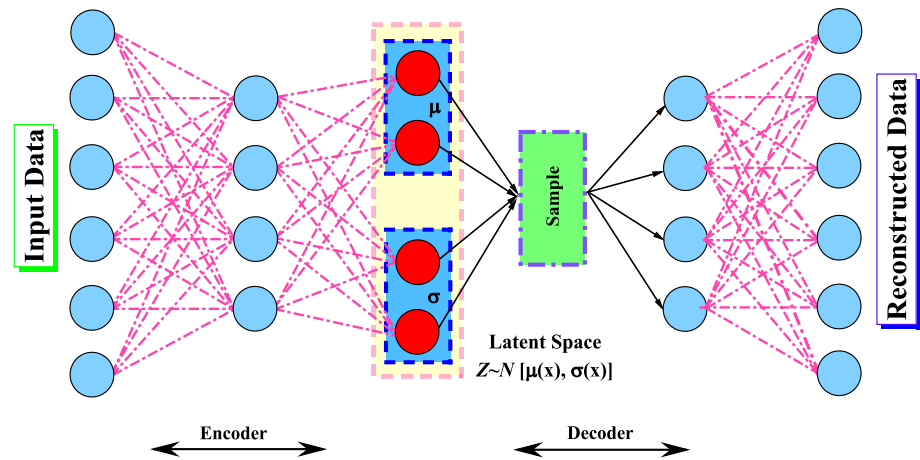


Fig. 8 Architecture of GANs and the procedure used for data generation

overall quality of the dataset for subsequent analysis. Using this method provided the lack of data input features and improved the datasets.

However, still the number of datasets can be an affective factor for the performance of ML models. Therefore, due to a smaller number of available datasets, synthetic data generation methods such as VAEs and GANs as illustrated in Figs. 7 and 8 have been used to learn the underlying distribution of real data and generate new, similar data points. These two approaches can widely help data scientist to generate and increase data numbers in a proper procedure to avoid any data preparation issues of overfitting or underfitting. Therefore, using these two approaches can increase the performance of ML models while can help the small dataset to be used for ML models [63].

3.3 Feature selection method

One of the most reliable feature selection methods is using the Heatmap graph that illustrates the correlations between the input features and outputs. While there are numbers of input features, this can help to reduce the number of inputs without reduction on the accuracy. However, redundant input feature can affect the performance

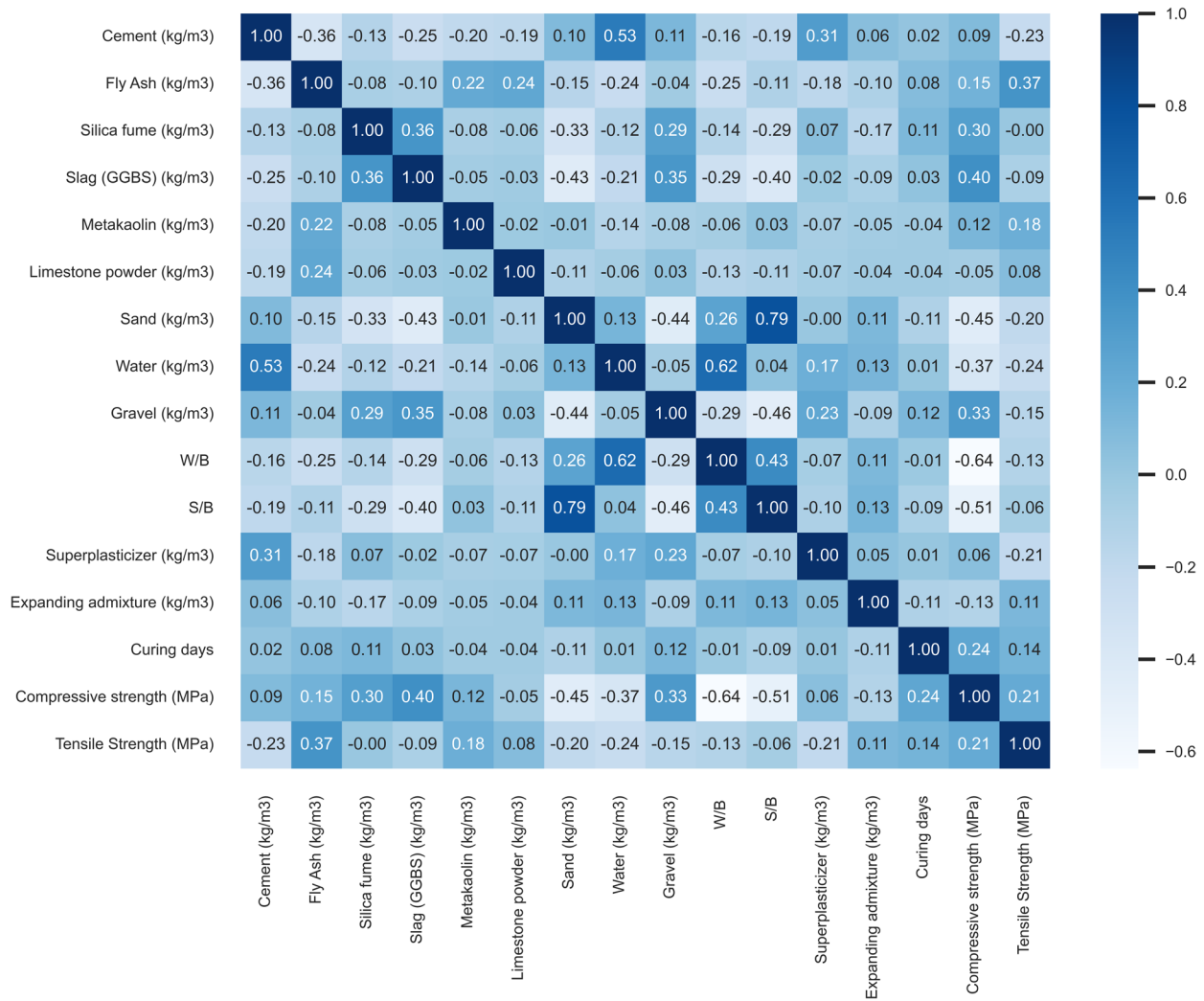


Fig. 9 Heatmap presentation for PAC dataset.

of ML model and should be neglected. Figures 9, 10 and 11 present the Heatmap for PAC and FR-PAC datasets, respectively. According to Figs. 9 and 10 there is a strong positive correlation (0.62) between the W/B ratio and water content, which is expected as the water content directly influences the W/C ratio. The W/C ratio has a strong negative correlation with compressive strength (-0.64), indicating that higher water content relative to cement tends to weaken the PAC. GGBS shows a strong positive correlation with sand (0.79), suggesting that mixes with higher GGBS content might also have higher sand content. Both GGBS and sand have a moderate negative correlation with compressive strength (-0.40 and -0.45, respectively), suggesting that higher amounts may reduce compressive strength. The superplasticizer has a positive correlation with compressive strength (0.24) and a moderate positive correlation with water content (0.17), which indicates that its use can improve workability without compromising strength significantly. Silica fume has a moderate positive correlation with compressive strength (0.30), suggesting it contributes positively to the strength of the concrete. FA shows a moderate positive correlation with tensile strength (0.37), indicating that FA may contribute to the tensile properties of the concrete mix. There is a positive correlation between curing days and both compressive (0.24) and tensile strength (0.14), emphasizing the importance of adequate curing time for achieving strength in concrete. Limestone powder shows very little correlation with compressive strength (0.08) and a slight negative correlation with tensile strength (-0.15), suggesting it does not significantly affect the strength properties of concrete. Whereas, water content has

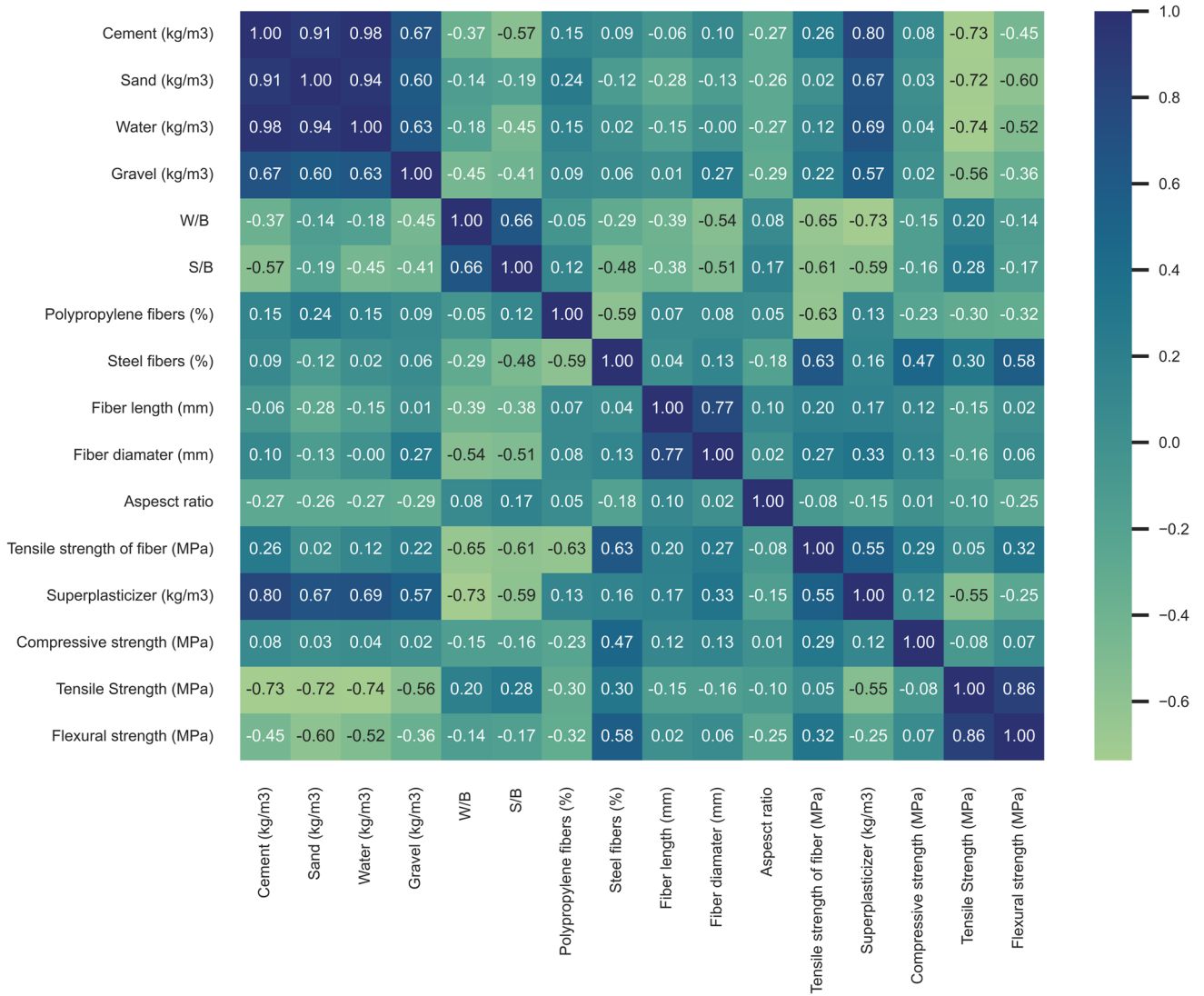
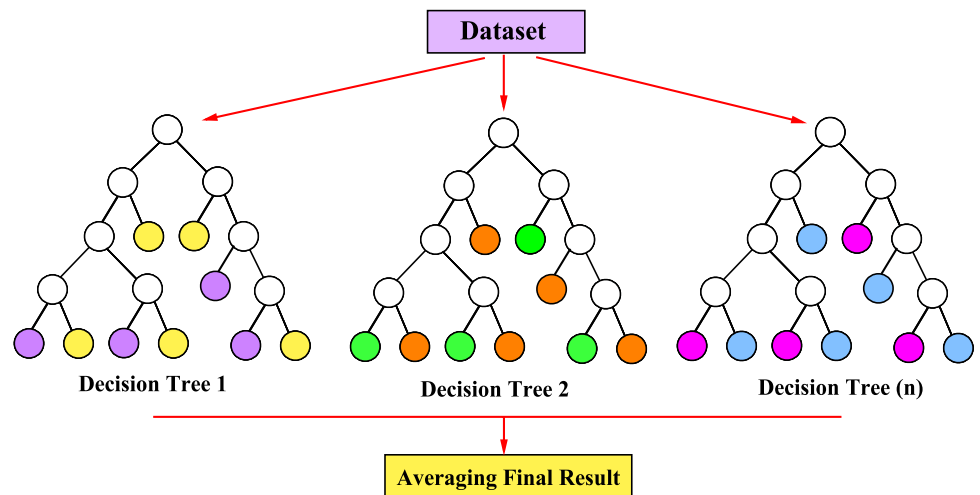


Fig. 10 Heatmap presentation for FR-PAC dataset

Fig. 11 Illustration of RF model



a strong positive correlation with compressive strength (0.53), which could be due to its relationship with workability and the hydration process, although it typically reduces strength when W/C ratios are high

According to Fig. 11, there are very strong positive correlations among cement, sand, and water contents, with coefficients above 0.90 that indicate these components are typically proportioned together in the mix designs and no possibility to neglect them in the dataset. Gravel content has a moderate positive correlation with water (0.63) and a moderate negative correlation with W/B ratio (− 0.45) and S/B ratio (− 0.41), suggesting that higher gravel content may be associated with lower W/B and S/B ratios. The W/B ratio has strong negative correlations with the tensile strength of fiber (− 0.65) and compressive strength (− 0.73), indicating that higher W/B ratios may detrimentally affect these strength properties. Steel fibers show a strong positive correlation with a tensile strength of fiber (0.63) and a moderate positive correlation with flexural strength (0.58), suggesting steel fibers contribute to the strength of the FR-PAC. Polypropylene fibers have a moderate positive correlation with water (0.15) but a weak relationship with strength properties. Fiber diameter shows a strong positive correlation with fiber length (0.77) and a moderate positive correlation with the aspect ratio (0.27). However, fiber length and diameter have weak correlations with mechanical properties, suggesting they may not be the dominant factors affecting strength. The aspect ratio of fibers has weak correlations with mechanical properties, indicating that it might not be a significant factor in predicting strength outcomes within the dataset. There is a strong positive correlation between superplasticizer content and water content (0.57), and a strong negative correlation with W/B (− 0.73), suggesting that superplasticizer is used to improve workability without increasing the W/B ratio. Superplasticizer also has a strong positive correlation with a tensile strength of fiber (0.55), which may indicate an improved distribution and effectiveness of fibers in the mix. Compressive strength has a moderate positive correlation with fiber tensile strength (0.47) and a strong negative correlation with W/B (− 0.74). Tensile strength shows a very strong positive correlation with flexural strength (0.86), which is expected as these properties are related to the material’s ability to resist cracking and breaking under tension. Flexural strength is moderately correlated with steel fibers (0.58), indicating that steel fibers help improve the flexural capacity of the FR-PAC.

By preparing the datasets according to literature, there is a possibility to have a wide range of input features included in the ML model and this can enhance its ability to include any effective parameter. Tables 8 and 9

Table 8 Data information of PAC dataset

Metric	Cement (kg/m ³)	Fly ash (kg/m ³)	Silica fume (kg/m ³)	Slag (GGBS) (kg/m ³)	Metakaolin (kg/m ³)	Limestone powder (kg/m ³)	Sand (kg/m ³)	Water (kg/m ³)
Mean	412.09	99.15	13.33	140.56	20.34	127.08	364.87	228.68
Std	144.88	12.86	5.97	3.81	0.36	25.96	116.78	80.06
Min	20.79	56.70	0.05	126.11	19.16	26.83	1.91	2.09
25%	345.99	91.86	10.32	138.60	20.10	113.14	297.19	177.99
50%	412.22	96.45	13.41	139.80	20.30	126.84	382.81	215.80
75%	468.71	103.64	15.72	141.72	20.53	142.58	444.70	267.88
Max	955.67	185.98	49.77	165.45	21.80	229.44	668.89	533.90
Metric	Gravel (kg/m ³)	W/B	S/B	Superplasticizer (kg/m ³)	Expanding admixture (kg/m ³)	Curing days	Compressive strength (MPa)	Tensile strength (MPa)
Mean	1489.07	0.52	0.97	6.36	8.07	19.00	18.99	2.21
Std	119.99	0.17	0.29	2.19	0.46	15.56	6.89	0.92
Min	1194.97	0.06	0.07	0.04	6.05	0.00	0.00	0.01
25%	1425.91	0.41	0.80	5.26	7.84	8.53	14.81	1.63
50%	1465.10	0.48	0.96	6.73	8.04	15.02	18.82	2.08
75%	1514.62	0.58	1.11	7.83	8.32	23.87	22.60	2.78
Max	2331.01	1.71	2.49	13.34	9.87	95.33	43.92	5.38

Table 9 Data information of FR-PAC dataset

Metric	Cement (kg/m ³)	Sand (kg/m ³)	Water (kg/m ³)	Gravel (kg/m ³)	W/B	S/B	Polypropylene fibers (%)	Steel fibers (%)
Mean	798.92	783.70	352.29	1447.87	0.44	0.98	1.86	2.99
Std	42.73	60.99	24.26	12.58	0.01	0.06	0.20	0.99
Min	724.19	500.30	312.31	1412.51	0.41	0.53	1.66	0.79
25%	775.80	767.70	338.71	1440.69	0.44	0.99	1.77	2.33
50%	795.52	800.06	344.07	1446.51	0.44	1.00	1.81	2.83
75%	813.24	817.17	358.42	1452.55	0.45	1.01	1.87	3.35
Max	1213.85	993.98	540.34	1557.97	0.57	1.07	4.25	8.48
Metric	Fiber length (mm)	Fiber diameter (mm)	Aspect ratio	Tensile strength of fiber (MPa)	Superplasticizer (kg/m ³)	Compressive strength (MPa)	Tensile strength (MPa)	Flexural strength (MPa)
Mean	36.20	0.64	54.13	1237.99	4.35	41.13	5.25	5.43
Std	12.76	0.22	9.91	201.74	0.42	6.20	0.38	0.37
Min	0.08	0.00	10.11	33.10	3.20	27.54	3.51	3.40
25%	29.60	0.49	49.02	1176.66	4.05	37.86	5.13	5.32
50%	31.48	0.54	57.27	1245.52	4.30	40.82	5.27	5.52
75%	44.28	0.79	60.36	1349.71	4.62	42.48	5.42	5.61
Max	92.07	1.82	82.81	1671.72	6.43	92.84	6.98	8.62

Table 10 Evaluation indicators are used for assessing ML models [64]

Evaluation indicator	Description
Coefficient of determination	$R^2 = 1 - \frac{\sum_{i=1}^n (\text{Actual}_i - \text{Predicted}_i)^2}{\sum_{i=1}^n (\text{Actual}_i - \text{Actual}_{\text{avg}})^2}$
Mean squared error	$\text{MSE} = \frac{1}{n} \sum_{i=1}^n (\text{Actual}_i - \text{Predicted}_i)^2$
Mean absolute error	$\text{MAE} = \frac{1}{n} \sum_{i=1}^n \text{Actual}_i - \text{Predicted}_i $
Mean absolute relative error	$\text{MARE} = \frac{1}{n} \sum_{i=1}^n \left \frac{\text{Actual}_i - \text{Predicted}_i}{\text{Actual}_i} \right $
Mean square relative error	$\text{MSRE} = \frac{1}{n} \sum_{i=1}^n \left \frac{\text{Actual}_i - \text{Predicted}_i}{\text{Actual}_i} \right ^2$
Root mean squared relative error	$\text{RMSRE} = \sqrt{\frac{1}{n} \sum_{i=1}^n \left(\frac{\text{Actual}_i - \text{Predicted}_i}{\text{Actual}_i} \right)^2}$
Mean bias error	$\text{MBE} = \frac{1}{n} \sum_{i=1}^n (\text{Actual}_i - \text{Predicted}_i)$
Maximum absolute relative error	$\text{erMAX} = \max \left(\left \frac{\text{Actual}_i - \text{Predicted}_i}{\text{Actual}_i} \right \right)$
Standard deviation	$\text{SD} = \sqrt{\frac{\sum (X_i - \text{Arithmetic mean})^2}{\text{total number}}}$

present the information on PAC and FR-PAC datasets, respectively. According to tables, the prepared datasets have a good range of spread and can include a reasonable range of inputs. Moreover, for a better comparison of ML models and their performance, the evaluation metrics of Table 10 were used.

Fig. 12 Illustration of GBM model

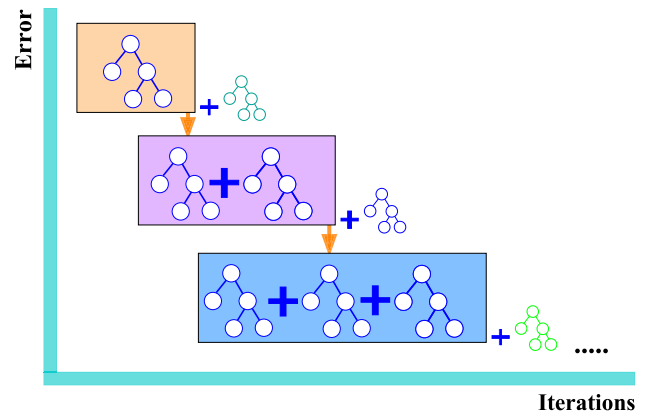
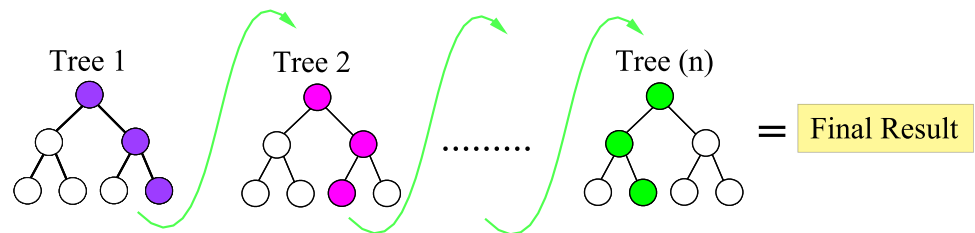


Fig. 13 Illustration of XGBoost model



4 Proposed ensemble ML model

In this section, the proposed optimization-based multi-target stacked ML models is introduced, which different stacked ML models are considered for estimating the mechanical strengths of PAC and FR-PAC. As it is clear from the Heatmap of datasets, there is correlation between mechanical strengths and this means there is a positive influence on using the predicted output as an input feature for the next output. Therefore, the optimization-based multi-target stacked ML model is proposed with the automated ability that improved the accuracy of the predictions.

Seven conventional ML models of RF, GBM, XGBoost, LightGBM, ETR, BR, and KNN were chosen for their individual strengths and predictive capabilities. Each of these models brings a different approach to the problem, capturing various aspects of the data’s complexity. For instance, tree-based models like RF as depicted in Fig. 11, GBM as depicted in Fig. 12, and XGBoost as depicted in Fig. 13, are known for handling non-linearity well, while BR can provide probabilistic insights. To optimize the performance of these base models, hyperparameter optimization algorithms like GWO, PSO, and NSPSO are employed, which they were implemented in a small number of random datasets to avoid higher execution time [65]. These optimization techniques search the hyperparameter space to find the settings that yield the best model performance, balancing between model complexity and generalization ability.

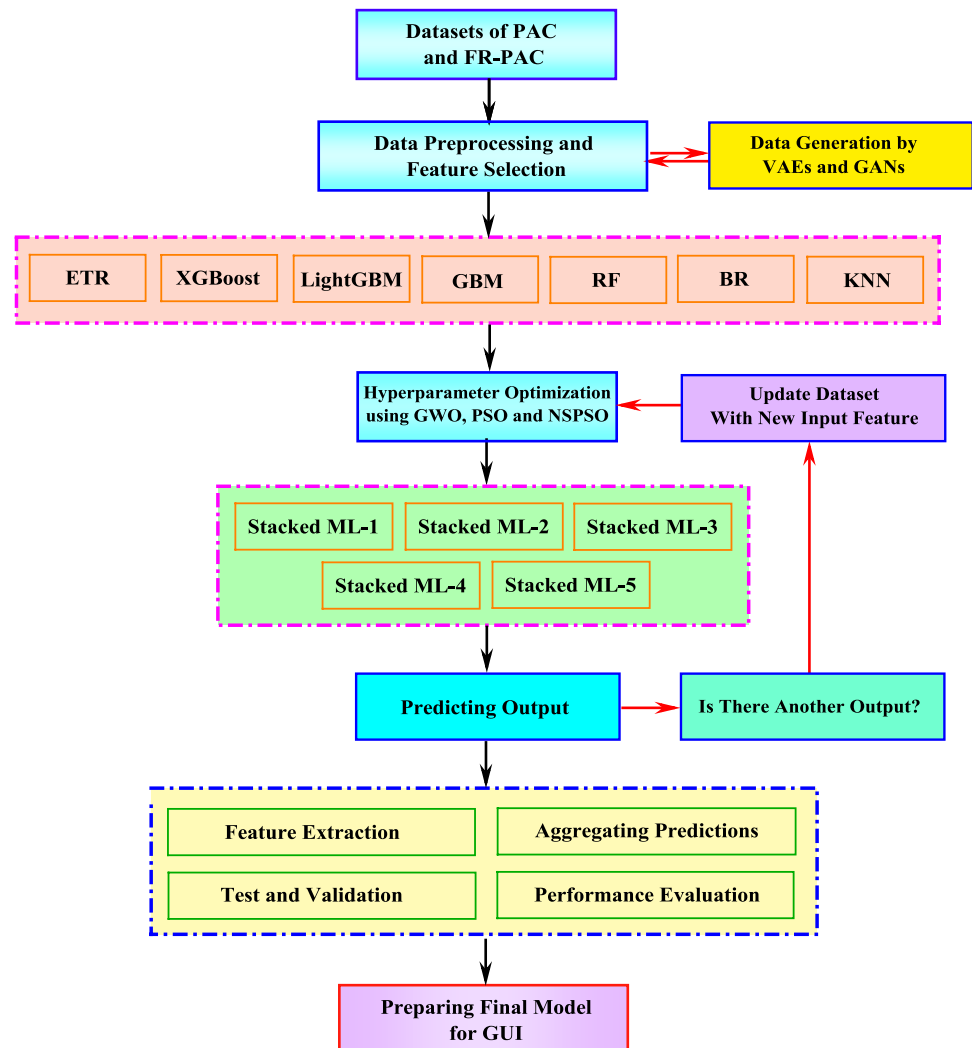
For developing stacked ML models, various algorithms and ML models can work together to improve overall predictive power and accuracy of system. The procedure begins with datasets such as PAC and FR-PAC, which are first subjected to data pre-processing and feature selection and then improved by VAEs and GANs. This step ensures that the models are trained on clean and relevant data, improving their ability to learn meaningful patterns. Once the base models are tuned, they are used to create stacked ML models as combination of different number of base learners. Stacking is an ensemble technique where the predictions from different base models are used to effectively capture the collective insights of the base models. This can lead to more accurate and robust predictions, as the stacked model can learn to correct the mistakes of individual base models. The stacked models then predict the outputs in a sequence, where each predicted target was added back into the dataset as a new feature for predicting the next target. This iterative approach allows the

models to learn the interdependencies between the targets, as the prediction for one target can provide valuable context for another (see correlation Heatmap between the targets). Predictions from different models in the sequence are aggregated to form the final output for each target. The predictions represent an aggregated result from various models, smoothing out individual errors and improving the confidence in the predictions. The model is then rigorously tested and validated on unseen data to ensure that it generalizes well beyond the training dataset [66]. Performance evaluation metrics are used to assess the model's accuracy, reliability, and predictive power, guiding any necessary refinements.

Ultimately, the final model (i.e., the best-stacked ML model) is prepared for practical deployment, which can include the integration into a GUI for user-friendly access. Figure 14 illustrates the multi-output stacked ML models for estimating different mechanical properties of PAC and FR-PAC. After careful evaluation of different combinations for stacked ML models, only five stacked ML algorithms were selected as follows:

- *Stacked ML-1*: a combination of BR, XGBoost, and GBM in a parallel execution,
- *Stacked ML-2*: a combination of BR, ETR, and RF in a parallel execution,
- *Stacked ML-3*: a combination of ETR, RF, KNN, XGBoost, and GBM in a parallel execution,
- *Stacked ML-4*: a combination of LGBM, XGBoost, and GBM in a parallel execution, and
- *Stacked ML-5*: a combination of RF, XGBoost, and GBM in a parallel execution.

Fig. 14 Multi-output stacked ML models for estimating different mechanical properties of PAC and FR-PAC



4.1 Hyperparameter tuning

By providing different types of inputs and increasing input features by adding the output in each part of the prediction, it is hard to modify the hyperparameters and tuned them based on the new condition. As illustrated in Fig. 14, the proposed ML models are hyperparameter free and can be tuned by innovative approached of GWO, PSO, and NSPSO, which can help to automate the total procedure [65]. Each of the optimization methods can be utilized effectively within the procedure to fine-tune hyperparameters. However, a significant challenge is the high execution time associated with these methods, especially when dealing with large datasets (i.e., datasets were increased using VAEs and GANs). To address this, a smaller randomly selected dataset was used for the initial tuning process [67]. This smaller dataset was chosen to represent the larger dataset's key characteristics while significantly reducing the computational time. By tuning the hyperparameters on this reduced dataset, the optimization process became more manageable and time-efficient. Once the optimal hyperparameters were identified using the smaller dataset, they were then applied to the full dataset, ensuring that the benefits of optimization were considered without increasing computational time. This approach balances the need for thorough hyperparameter tuning with the practical constraints of execution time, ultimately enhancing the efficiency and effectiveness of the proposed stacked ML models.

4.1.1 Grey wolf optimizer

The GWO is a sophisticated algorithm that emulates the leadership hierarchy and hunting mechanism of grey wolves in the wild. This algorithm has gained acceptable results for its efficacy in hyperparameter optimization of ML models due to its balance between exploration and exploitation in search space. GWO models categorizing grey wolves into four groups of α , for the best candidate solution that is responsible for decision-making, β , for the second-best solution, which assists the alpha and maintains the hierarchy, δ , for the third-best solution, which follows the alpha and beta, and ω , for the remaining solutions, which follow the top three and help in exploring the search space [65]. To use GWO for hyperparameter optimization, first the search space should be defined. Then, GWO randomly generates an initial population of grey wolves, each representing a different set of hyperparameters, and trains the ML model using the hyperparameters of each grey wolf and evaluate its performance based on a chosen metric (e.g., accuracy, loss). Afterwards, the GWO updates the positions of the wolves based on the fitness evaluations, iteratively refining the search for optimal hyperparameters and will continue the iterations until a stopping criterion is met (e.g., maximum iteration number or a satisfactory performance level) [16]. The proposed GWO can select small random data points of the dataset to optimize the hyperparameters while it reduces the execution time. This ability improved its performance and provided reasonable results.

4.1.2 Particle swarm optimization

PSO is widely used for hyperparameter optimization in ML due to its simplicity, ease of implementation, and efficiency in converging to optimal solutions. In PSO, a swarm consists of a number of particles, each representing a potential solution in the search space of hyperparameters. The PSO algorithm begins by initializing a swarm of particles. Each particle has a position to represents a set of hyperparameters, and velocity to determine the direction and distance the particle that will move in the next iteration. The best position of the particle is assumed as the personal best position, P_{best} , and the best position of any particle in the swarm is assumed as the global best position G_{best} . The core of PSO lies in updating the velocity and position of each particle [65]. This is influenced by both the particle's own best experience and the swarm's best experience. PSO balances exploration and exploitation through the inertia weight, in other words, higher inertia weight increase search space exploration and lower weight promotes exploitation of known good solutions. Although

the GWO was the best optimizer in some of the stacked ML models, PSO showed higher results and was employed as optimization tool other stacked ML models.

4.1.3 Non-dominated sorting PSO

To improve the capability of PSO, NSPSO, which is an advanced variant of the PSO algorithm, designed to work on multi-objective optimization problems. Since in stacked ML models there are a combination of different types of hyperparameters, the search space should be defined for each of the spaces and the optimized value for each hyperparameter could affect other performance. Therefore, using NSPSO extends the basic PSO by incorporating concepts of Pareto dominance and non-dominated sorting, making it particularly effective for hyperparameter optimization in scenarios where multiple conflicting objectives need to be considered. Pareto dominance is used to compare solutions. Similar to PSO, after updating positions and velocities, particles are evaluated based on multiple objectives. Non-dominated sorting is performed to classify particles into different Pareto fronts. The algorithm prioritizes selecting particles from the lower-order fronts, ensuring a diverse set of high-quality solutions. Finally, it continues updating velocities, positions, and best positions, and performing non-dominated sorting for a predetermined iteration number or until convergence, criteria are met.

5 Estimating mechanical properties of PAC

In this section, the results of proposed stacked ML models on two datasets of PAC and FR-PAC are discussed. Different methods were used to have the highest percentage of predictions on the test dataset, which was assumed 20% of the total dataset.

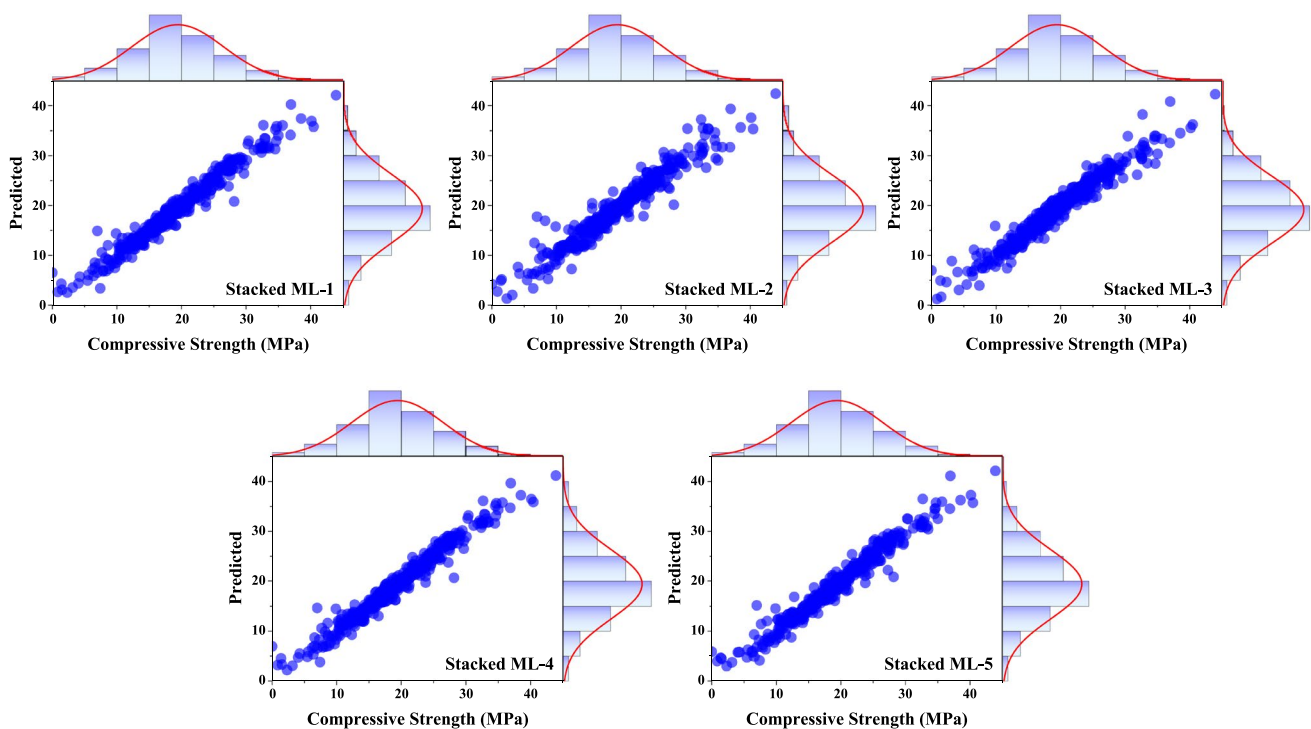


Fig. 15 Scatter plot presentation of compressive strength of PAC using stacked ML models

5.1 Prediction results of PAC

Figure 15 illustrates scatter graphs of PAC compressive strength using stacked ML models. The scatter plot presentation consists of five individual scatter plots, each depicting the predicted versus actual compressive strength (determined in literature) for PAC using different stacked ML models, as labelled stacked ML-1 through stacked ML-5. All five models show a strong positive correlation between predicted and actual compressive strengths, as the majority of data points are clustered close to a hypothetical diagonal line of $x=y$. They have a good distribution along this line that confirms the acceptable accuracy of proposed ML models. Histograms are also included on the top and right sides of each scatter plot, representing the distribution of actual and predicted values, respectively. These histograms show how the predictions and actual values are spread across different strength levels. While comparing those histograms, it is clear that the distribution of actual and estimated compressive strength of PAC is similar and confirms the capability of stacked ML models. Similarly, Fig. 16 shows scatter graphs of the tensile strength of PAC using stacked ML models. All five models demonstrate a strong positive correlation between predicted and actual tensile strengths, indicated by the concentration of data points along the $x=y$ line where the predicted values would equal the actual values, suggests that the models are providing accurate predictions of the tensile strength of PAC. The density and alignment of the points along the diagonal in all five scatter plots suggest that each of the stacked ML models has a similar level of accuracy (i.e., more than 95%) in estimating the tensile strength of PAC.

To better present the results of stacked ML models, Table 11 was provided to illustrate prediction metrics of mechanical properties of PAC. As it is clear in the prediction of compressive strength, stacked ML-4 had the highest R^2 value (0.964), indicating the best proportion of variance explained. It also had the lowest MSE (1.78) and RMSE (1.34), showing the smallest average squared errors; Moreover, it performs best with the lowest MAE (0.95), which means it has the lowest average magnitude of errors. However, stacked ML-1 had the lowest MARE (0.072) and MSRE (0.036), suggesting it provides the most accurate predictions relative to the actual values and has the lowest RRMSE (0.018). For predicting tensile strength, stacked ML-5 and stacked ML-4 had the highest

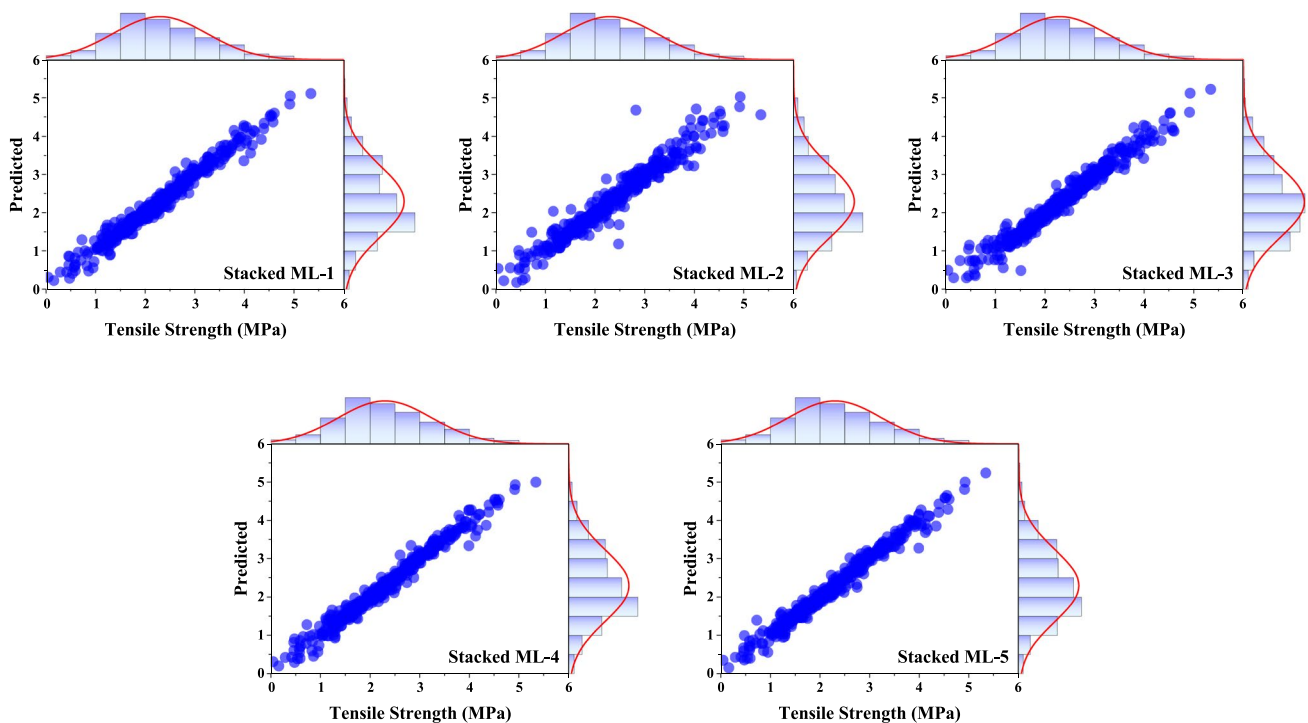


Fig. 16 Scatter plot presentation of tensile strength of PAC using stacked ML models

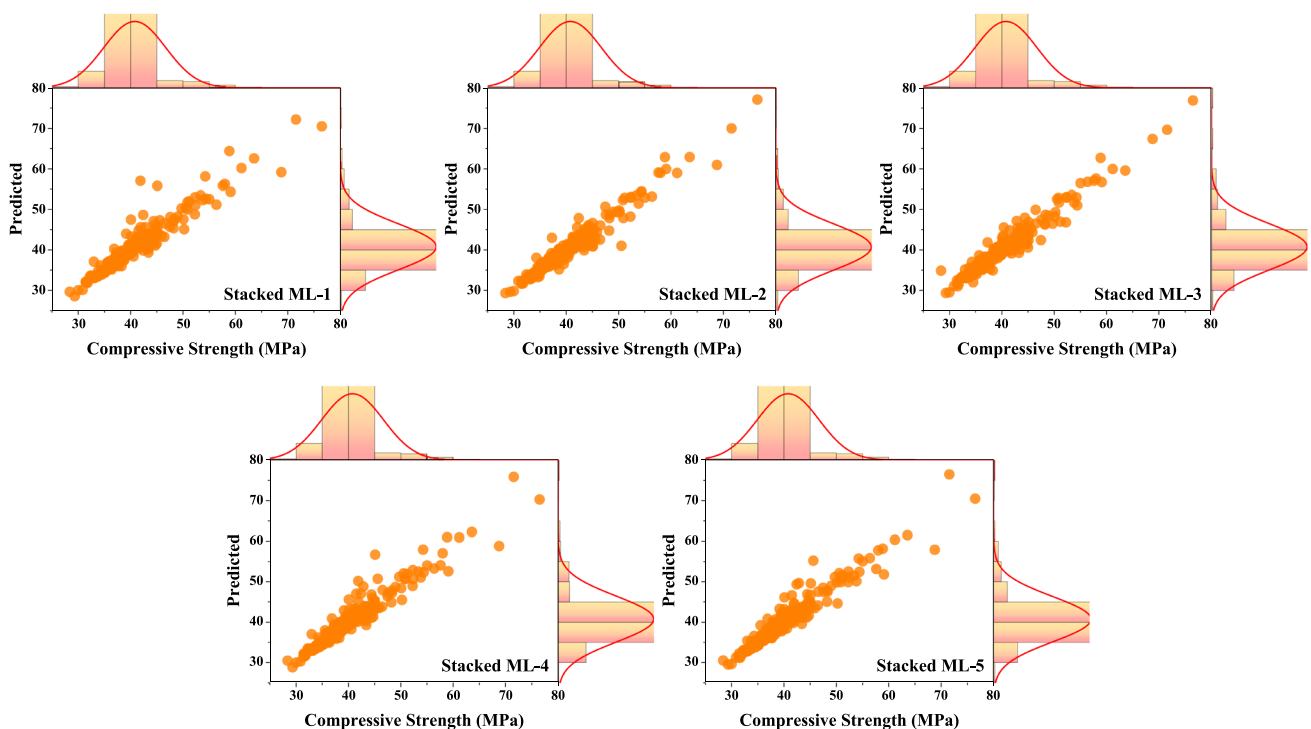
Table 11 Prediction metrics of mechanical properties of PAC using stacked ML models

ML algorithm	R^2	MSE	RMSE	MAE	MARE	MSRE	RMSRE	RRMSE	MBE	erMAX	SD
<i>Compressive strength</i>											
Stacked ML-1	0.963	1.86	1.36	0.98	0.072	0.036	0.191	0.018	0.016	2.168	1.36
Stacked ML-2	0.867	6.62	2.57	1.38	0.108	0.106	0.325	0.033	0.005	3.724	2.58
Stacked ML-3	0.955	2.57	1.60	1.15	0.080	0.039	0.198	0.021	0.228	2.592	1.59
Stacked ML-4	0.964	1.78	1.34	0.95	0.072	0.046	0.216	0.017	0.016	2.801	1.34
Stacked ML-5	0.958	2.11	1.45	1.02	0.082	0.072	0.267	0.019	0.016	3.739	1.45
<i>Tensile strength</i>											
Stacked ML-1	0.974	0.02	0.15	0.11	0.081	0.112	0.335	0.016	0.0	6.240	0.15
Stacked ML-2	0.941	0.05	0.23	0.15	0.111	0.365	0.604	0.025	0.007	11.650	0.23
Stacked ML-3	0.964	0.03	0.18	0.13	0.106	0.312	0.558	0.020	0.019	10.614	0.18
Stacked ML-4	0.976	0.02	0.15	0.10	0.078	0.112	0.335	0.016	0.0	6.254	0.15
Stacked ML-5	0.977	0.02	0.14	0.10	0.078	0.139	0.373	0.016	0.0	7.102	0.14

R^2 value (0.977 and 0.976, respectively) with approximately the same error metric values. As it is presented, stacked ML-1, stacked ML-3, stacked ML-4 and stacked ML-5 had an accuracy of predictions higher than 95.5% which shows their superior performance. The results also present superior accuracy compared to the previous study (see [32]) compared to conventional ML models.

5.2 Prediction results of FR-PAC

Figures 17, 18, and 19 present scatter plots of compressive, flexural and tensile strengths of FR-PAC using stacked ML models, respectively. The results demonstrate that all the proposed stacked ML models exhibited predictions closely aligned with the $x = y$ line, which indicates a high degree of accuracy and reliability. The $x = y$ line

**Fig. 17** Scatter plot presentation of compressive strength of FR-PAC using stacked ML models

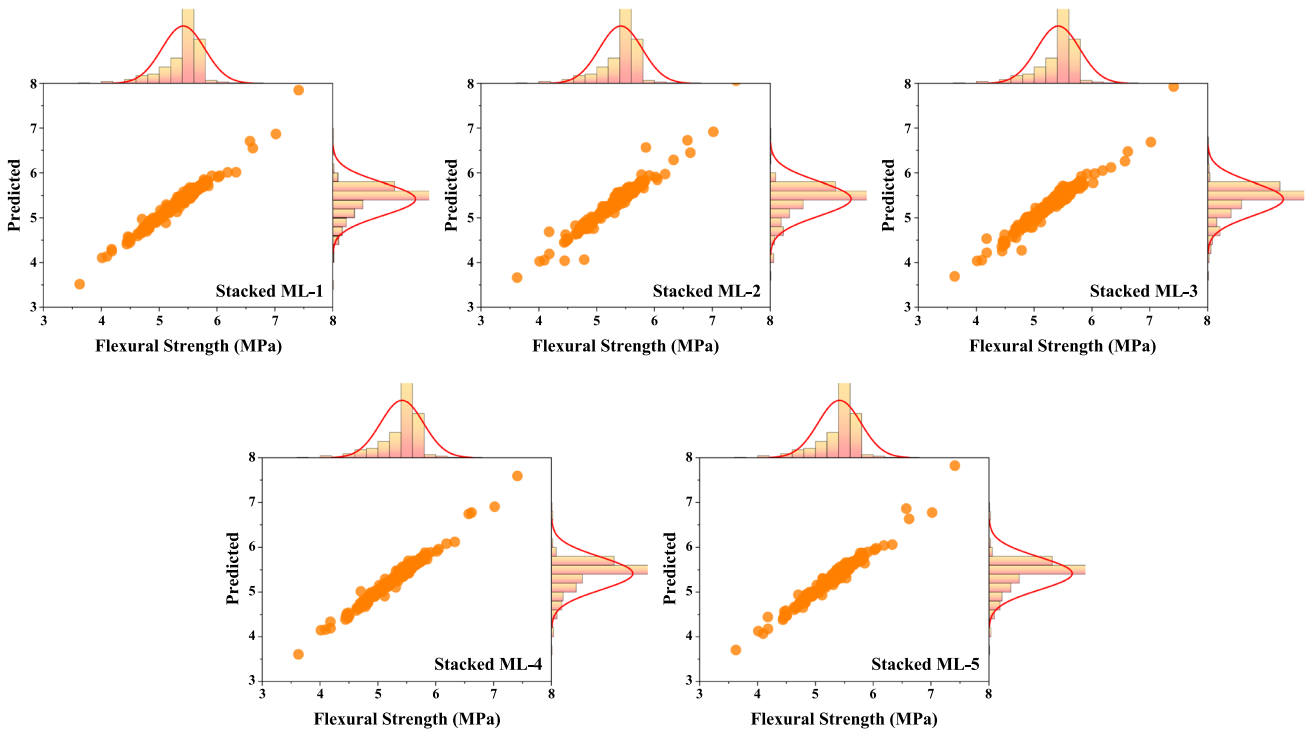


Fig. 18 Scatter plot presentation of flexural strength of FR-PAC using stacked ML models

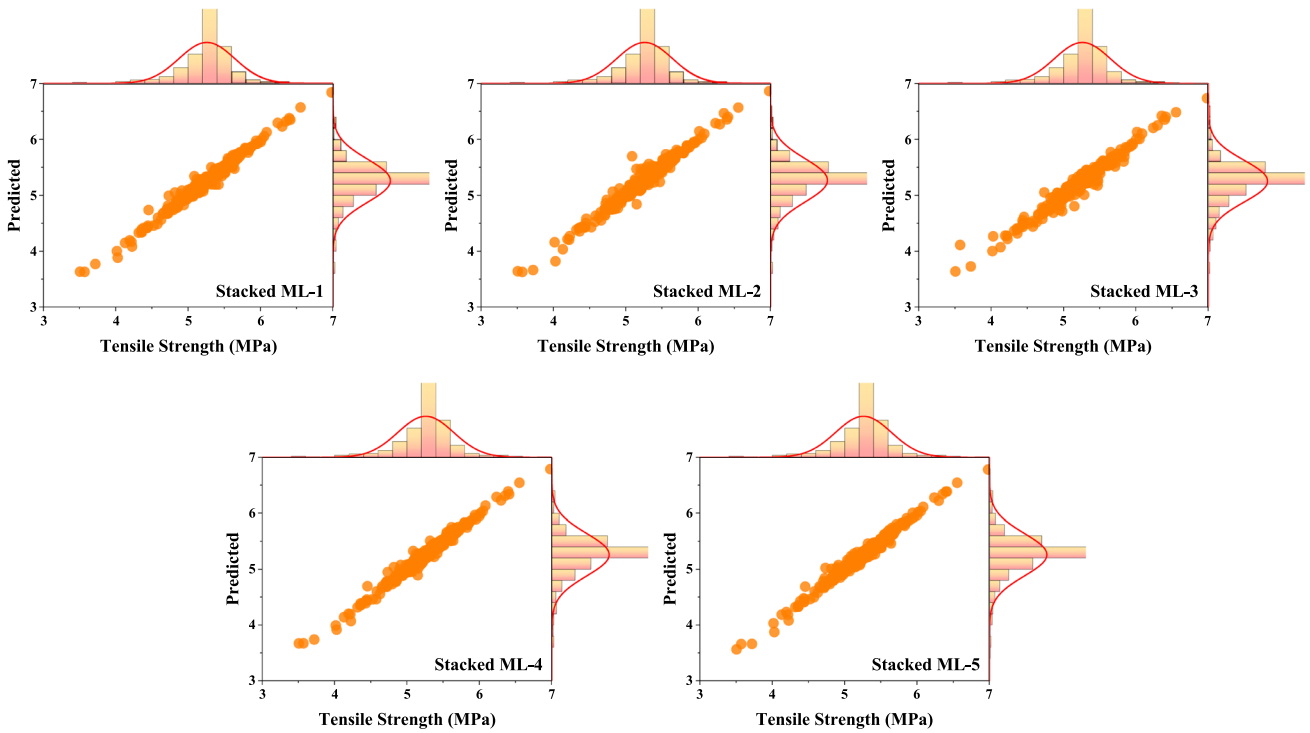


Fig. 19 Scatter plot presentation of tensile strength of FR-PAC using stacked ML models

represents a perfect prediction scenario where the predicted values exactly match the observed values. Therefore, the proximity of the model predictions to this line is a strong indicator of their precision. This alignment suggests that the stacked ML models effectively captured the underlying patterns in the data, minimizing both bias and variance. The accuracy of these models can be attributed to the strategic combination of base learners within the stacking framework, which allows for a more comprehensive understanding of the data. Each base model contributes unique strengths, and the meta-learner optimally integrates these insights, leading to robust predictions. Moreover, the consistency of these results across different datasets or scenarios further validates the ML models' generalizability. This capability is crucial in practical applications, where models must perform reliably across varying conditions and data distributions. The stacked ML models' performance highlights their potential as powerful tools for predictive modeling, offering both accuracy and adaptability in complex real-world situations.

To better present the results of the proposed stacked ML models, Table 12 was provided to illustrate prediction metrics of mechanical properties of FR-PAC. Stacked ML-2 has the highest R^2 value of 0.956, indicating the best fit to the data. It also has the lowest MSE (1.54), RMSE (1.24), and MAE (0.67), showing it to be the most accurate and precise model for predicting the compressive strength of FR-PAC. The low MARE (0.016), MSRE (0.001), and RMSRE (0.028) further confirm this model's superior performance. Additionally, the erMAX (maximum relative error) is the lowest (0.188), indicating the highest reliability. Stacked ML-1 and stacked ML-4 also perform well but fall behind stacked ML-2 in almost all metrics. For example, Stacked ML-1 has a slightly lower R^2 of 0.923 and a higher RMSE (1.64) compared to stacked ML-2, similarly, stacked ML-4 has an R^2 of 0.930 but a higher MSE (2.46).

For flexural strength, stacked ML-4 achieved the highest R^2 value of 0.981, indicating the best fit for flexural strength data. It also has the lowest MSE (0.00), RMSE (0.05), MAE (0.03), and other related metrics, which suggests the highest accuracy in predictions. The minimal MARE (0.006) and RMSRE (0.010) reinforce this model's effectiveness. Stacked ML-1 and stacked ML-5 also perform well but are slightly less accurate than stacked ML-4. For instance, stacked ML-1 has a slightly lower R^2 of 0.976 and a slightly higher RMSE (0.06). For tensile strength, stacked ML-4 and stacked ML-5 both models have the highest R^2 values of 0.982, indicating excellent fits for tensile strength data. However, stacked ML-4 has a slightly lower RMSE (0.05) and MAE (0.03) compared to stacked ML-5, suggesting slightly better accuracy. Stacked ML-1 also performs well, with an R^2 of

Table 12 Prediction metrics of mechanical properties of FR-PAC using stacked ML models

ML algorithm	R^2	MSE	RMSE	MAE	MARE	MSRE	RMSRE	RRMSE	MBE	erMAX	SD
<i>Compressive strength</i>											
Stacked ML-1	0.923	2.69	1.64	0.81	0.019	0.001	0.037	0.010	0.0	0.363	1.64
Stacked ML-2	0.956	1.54	1.24	0.67	0.016	0.001	0.028	0.008	0.043	0.188	1.24
Stacked ML-3	0.893	3.76	1.94	0.86	0.021	0.002	0.046	0.012	0.102	0.568	1.94
Stacked ML-4	0.930	2.46	1.57	0.86	0.020	0.001	0.035	0.010	0.0	0.258	1.57
Stacked ML-5	0.919	2.82	1.68	0.86	0.020	0.001	0.037	0.010	0.0	0.322	1.68
<i>Flexural strength</i>											
Stacked ML-1	0.976	0.00	0.06	0.04	0.007	0.000	0.010	0.003	0.0	0.059	0.06
Stacked ML-2	0.945	0.01	0.09	0.04	0.008	0.000	0.016	0.004	0.008	0.151	0.09
Stacked ML-3	0.960	0.01	0.07	0.05	0.008	0.000	0.014	0.003	0.001	0.107	0.07
Stacked ML-4	0.981	0.00	0.05	0.03	0.006	0.000	0.010	0.002	0.0	0.066	0.05
Stacked ML-5	0.974	0.00	0.06	0.04	0.007	0.000	0.011	0.003	0.0	0.063	0.06
<i>Tensile strength</i>											
Stacked ML-1	0.980	0.00	0.05	0.04	0.007	0.000	0.011	0.003	0.0	0.064	0.05
Stacked ML-2	0.968	0.00	0.07	0.04	0.008	0.000	0.014	0.003	0.007	0.120	0.07
Stacked ML-3	0.963	0.01	0.07	0.05	0.009	0.000	0.015	0.004	0.008	0.151	0.07
Stacked ML-4	0.982	0.00	0.05	0.03	0.007	0.000	0.010	0.002	0.0	0.054	0.05
Stacked ML-5	0.982	0.00	0.05	0.04	0.007	0.000	0.010	0.002	0.0	0.061	0.05

0.980 and RMSE of 0.05, but falls just short of the precision offered by Stacked ML-4. In conclusion, stacked ML-4 is a highly reliable model, especially for predicting flexural and tensile strengths, while stacked ML-2 is superior in predicting compressive strength. The careful combination of base learners and meta-learning in these stacked models allows them to achieve high accuracy and robustness across different strength predictions.

6 Validation on generality of the stacked ML models

Validation of the generality of the stacked ML models is a critical step to ensure that the models can generalize well to new, unseen data, beyond the specific datasets on which they were trained and tested. The generality of an ML model refers to its ability to maintain high performance across a wide range of scenarios and data distributions, which is crucial for practical applications in engineering. In this section, different specimens of PAC and FR-PAC were experimentally tested and their results were determined as unseen dataset for assessing the generality of those proposed stacked ML models. In the following subsections, their results are discussed.

6.1 Experimental validation of stacked ML models for PAC

Figures 20 and 21 present a scatter plot of compressive and tensile strength of experimental specimens of PAC using stacked ML models, respectively. The results, as presented, indicate that the predictions exhibit a strong distribution along the $x = y$ line. This alignment suggests that the stacked ML models are making accurate predictions, as the predicted values closely match the actual values. The good spread along this line confirms the models' capability to generalize well across different scenarios, demonstrating both accuracy and reliability in the predictions. This alignment also implies that the models have successfully captured the underlying patterns in the data, leading to consistent performance across various metrics. Although the experimental data has been selected for validating dataset, the results of stacked ML models on the general dataset can confirm their superior accuracy of them and the procedure used for optimizing them on different types of datasets.

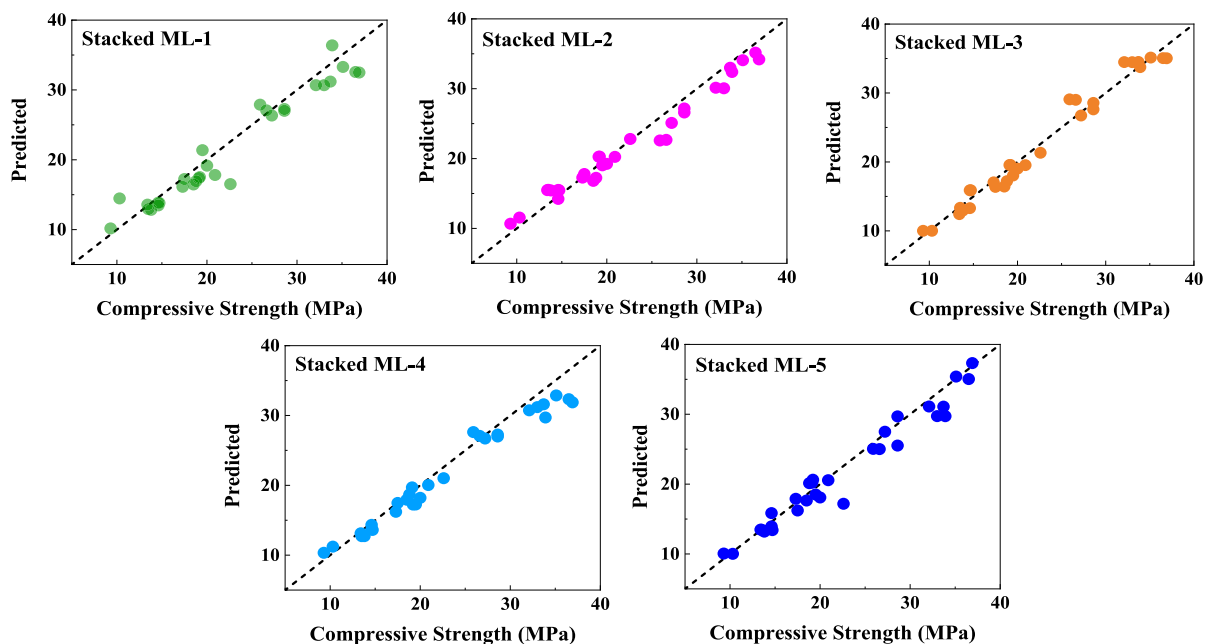


Fig. 20 Scatter plot presentation of compressive strength of experimental specimens of PAC using stacked ML models

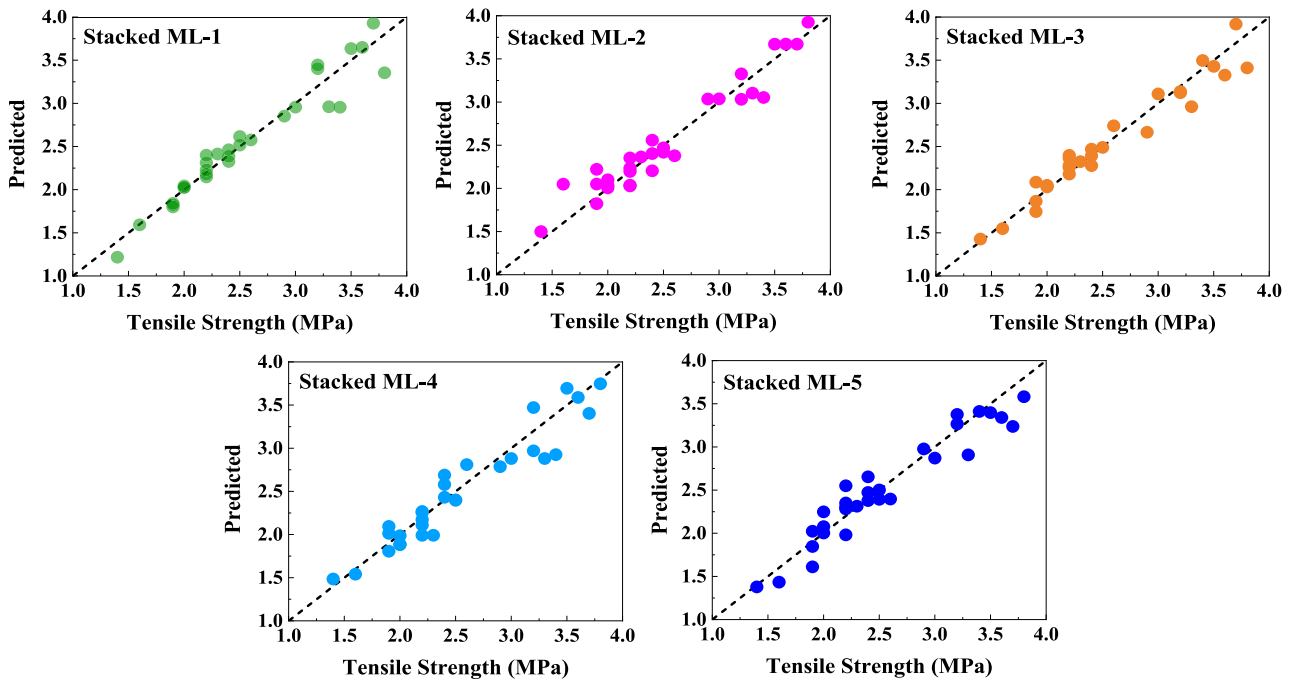


Fig. 21 Scatter plot presentation of tensile strength of PAC using stacked ML models

Table 13 Prediction metrics of mechanical properties of PAC using stacked ML models

ML algorithm	R^2	MSE	RMSE	MAE	MARE	MSRE	RMSRE	RRMSE	MBE	erMAX	SD
<i>Compressive strength</i>											
Stacked ML-1	0.957	2.91	1.71	1.44	0.069	0.007	0.082	0.259	0.589	0.155	1.63
Stacked ML-2	0.923	5.15	2.27	1.84	0.087	0.013	0.115	0.352	1.033	0.406	2.06
Stacked ML-3	0.948	3.51	1.87	1.45	0.062	0.005	0.072	0.292	1.133	0.136	1.52
Stacked ML-4	0.974	1.77	1.33	1.1	0.052	0.004	0.062	0.198	0.139	0.123	1.35
Stacked ML-5	0.951	3.29	1.81	1.34	0.059	0.006	0.075	0.278	0.767	0.24	1.67
<i>Tensile strength</i>											
Stacked ML-1	0.933	0.03	0.17	0.12	0.043	0.003	0.057	0.22	0.01	0.131	0.17
Stacked ML-2	0.911	0.04	0.19	0.15	0.06	0.005	0.071	0.256	0.042	0.139	0.19
Stacked ML-3	0.913	0.04	0.19	0.15	0.059	0.005	0.074	0.251	0.028	0.159	0.19
Stacked ML-4	0.933	0.03	0.17	0.13	0.056	0.006	0.078	0.217	0.019	0.281	0.17
Stacked ML-5	0.947	0.02	0.15	0.11	0.042	0.003	0.052	0.196	0.012	0.103	0.15

Moreover, the results of metrics presented in Table 13 show that the proposed stacked ML models exhibit strong predictive performance for both compressive and tensile strength. Stacked ML-4 emerges as the best-performing model for compressive strength with the highest R^2 value of 0.974, indicating the strongest correlation between predicted and actual values. It also exhibits the lowest error metrics, including MSE (1.77), RMSE (1.33), and MAE (1.10), which suggests that this model provides the most accurate and reliable predictions. Additionally, its MARE and RMSRE values are the lowest among the models, further validating its precision. For flexural strength, stacked ML-1 and stacked ML-5 also perform well, with R^2 values of 0.957 and 0.951, respectively. However, their error metrics are slightly higher than those of stacked ML-4, making them less optimal but still reliable options. Stacked ML-2 shows the weakest performance with an R^2 of 0.923 and the highest error metrics, including an MSE of 5.15 and RMSE of 2.27. This indicates that while it is still a valid model, its predictions are less accurate compared to the other models. For tensile strength, stacked ML-5 stands out as the most accurate

model for tensile strength predictions, with the highest R^2 value of 0.947 and the lowest MSE (0.02) and RMSE (0.15). This model also achieves the lowest MAE (0.11), indicating a high level of precision in its predictions. Stacked ML-1 and stacked ML-4 both have an R^2 value of 0.933, but stacked ML-1 offers slightly better error metrics, making it a slightly more reliable choice between the two. Stacked ML-2 and stacked ML-3 perform similarly, with both models having an R^2 value of 0.911 and 0.913, respectively. However, their higher error metrics compared to stacked ML-5 suggest they are less effective for tensile strength predictions. Overall, stacked ML-4 and stacked ML-5 is the best model for predicting compressive and tensile strengths of PAC due to its superior R^2 and lowest error metrics. Both models demonstrate strong generalization capabilities and reliability, making them the preferred choices depending on the specific mechanical property being predicted. The results confirm the superior accuracy of the proposed stacked ML models compared to conventional ML models investigated in [32], and outperform in reliability and generality of the predictive models.

6.2 Experimental validation of stacked ML models for FR-PAC

Figures 22, 23, and 24 present scatter plots of compressive, flexural, and tensile strengths of experimental specimens of FR-PAC using stacked ML models, respectively. The results indicate that the predictions exhibit a strong distribution along the $x = y$ line, which suggests that the models are accurately predicting the measured experimental values. Such a distribution is a hallmark of model reliability and precision, implying that the stacked ML models are capable of generalizing well across different samples of FR-PAC, thereby providing accurate predictions of material properties.

The results of the metrics presented in Table 14 show that the performance of the stacked ML models varies significantly across the different categories of compressive, flexural, and tensile strength of FR-PAC. For compressive strength, stacked ML-2 achieves the highest performance for compressive strength prediction with an impressive R^2 value of 0.986. This model also exhibits the lowest error metrics, including MSE (1.83), RMSE (1.35), MAE (1.11), MARE (0.038), and RMSRE (0.048). These low values indicate that stacked ML-2 provides highly accurate and reliable predictions for compressive strength. Stacked ML-4 and stacked ML-5 also demonstrate strong predictive capabilities, with R^2 values of 0.977 and 0.976, respectively. Although their error metrics are slightly higher than those of stacked ML-2, they still offer good accuracy, making them solid alternatives

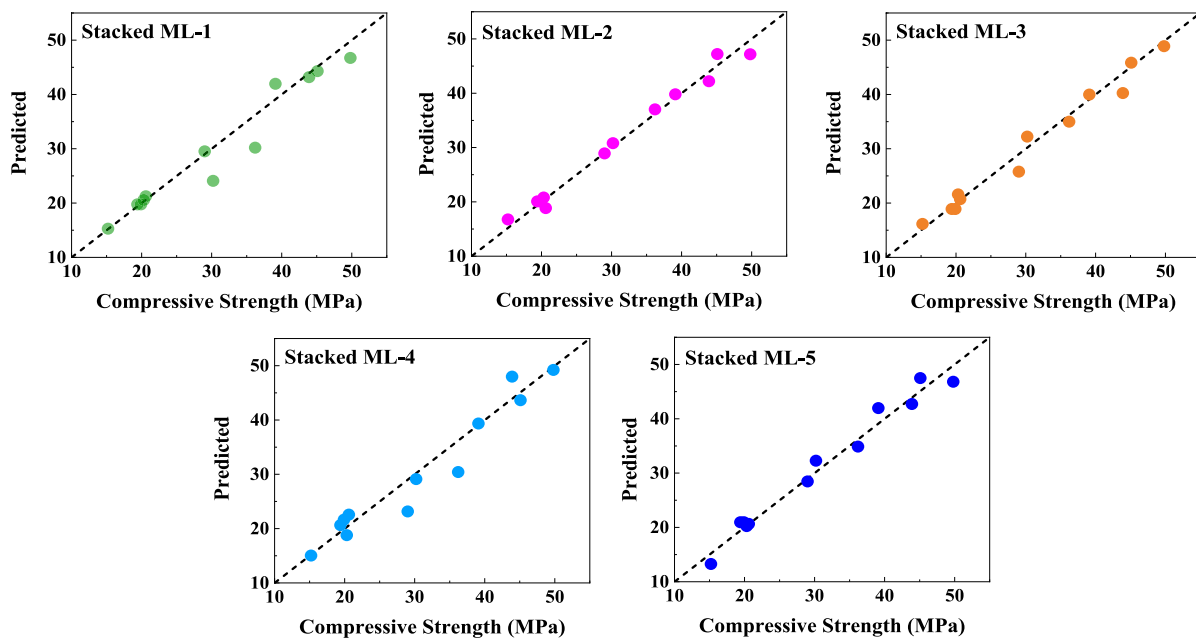


Fig. 22 Scatter plot presentation of compressive strength of FR-PAC using stacked ML models

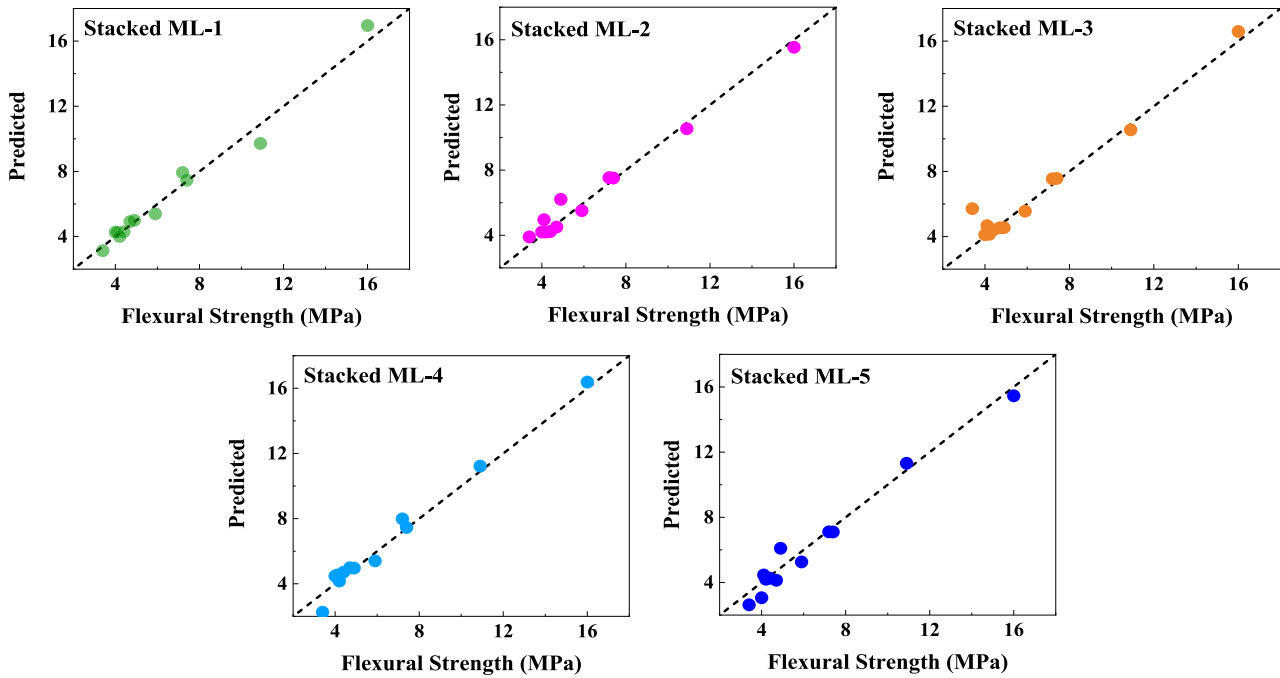


Fig. 23 Scatter plot presentation of flexural strength of FR-PAC using stacked ML models

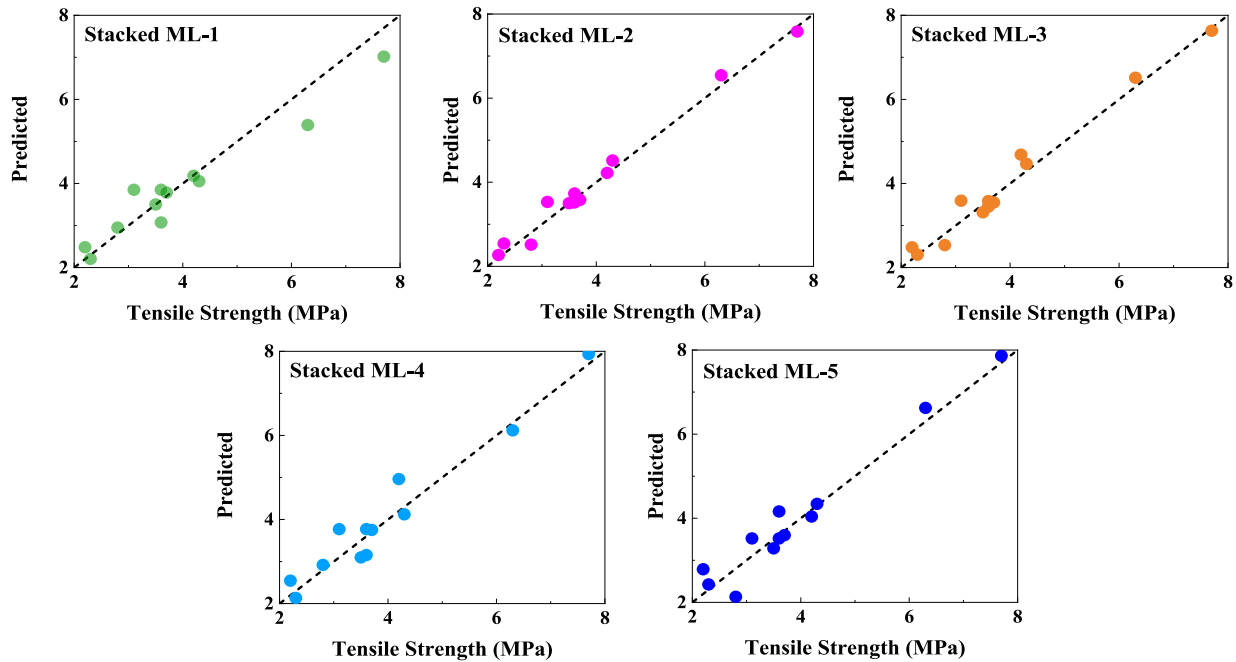


Fig. 24 Scatter plot presentation of tensile strength of FR-PAC using stacked ML models

for compressive strength prediction. Stacked ML- and stacked ML-3 have lower R^2 values (0.940 and 0.916, respectively) and higher error metrics, indicating less precise predictions. Specifically, stacked ML-3 shows the highest MSE (8.21) and RMSE (2.86), making it the least favorable model for compressive strength prediction.

On the other hand, for flexural strength, stacked ML-4 emerges as the best performer for flexural strength prediction of FR-PAC, with the highest R^2 value of 0.980. It also has the lowest error metrics, including MSE (0.25),

Table 14 Prediction metrics of mechanical properties of PAC using stacked ML models

ML algorithm	R^2	MSE	RMSE	MAE	MARE	MSRE	RMSRE	RRMSE	MBE	erMAX	SD
<i>Compressive strength</i>											
Stacked ML-1	0.94	7.74	2.78	1.8	0.053	0.007	0.082	0.78	1	0.202	2.71
Stacked ML-2	0.986	1.83	1.35	1.11	0.038	0.002	0.048	0.366	0.086	0.103	1.41
Stacked ML-3	0.916	8.21	2.86	2.14	0.073	0.009	0.093	0.792	0.583	0.201	2.93
Stacked ML-4	0.977	2.93	1.71	1.38	0.047	0.003	0.056	0.47	0.361	0.111	1.75
Stacked ML-5	0.976	3.15	1.77	1.5	0.05	0.004	0.061	0.479	0.167	0.127	1.85
<i>Flexural strength</i>											
Stacked ML-1	0.977	0.28	0.53	0.4	0.057	0.004	0.065	0.686	0.023	0.108	0.55
Stacked ML-2	0.977	0.29	0.54	0.41	0.079	0.013	0.112	0.679	0.146	0.267	0.54
Stacked ML-3	0.956	0.55	0.74	0.45	0.098	0.042	0.204	0.927	0.24	0.681	0.73
Stacked ML-4	0.980	0.25	0.5	0.4	0.081	0.014	0.118	0.638	0.121	0.336	0.51
Stacked ML-5	0.971	0.36	0.6	0.5	0.098	0.017	0.131	0.802	0.167	0.245	0.6
<i>Tensile strength</i>											
Stacked ML-1	0.939	0.14	0.38	0.31	0.089	0.012	0.11	0.781	0.083	0.217	0.38
Stacked ML-2	0.915	0.2	0.45	0.33	0.083	0.012	0.108	0.96	0.079	0.242	0.46
Stacked ML-3	0.946	0.13	0.36	0.29	0.09	0.015	0.124	0.736	0.083	0.267	0.36
Stacked ML-4	0.983	0.04	0.2	0.16	0.048	0.004	0.064	0.421	0.063	0.139	0.2
Stacked ML-5	0.972	0.07	0.26	0.21	0.06	0.006	0.078	0.532	0.068	0.158	0.26

RMSE (0.50), and MAE (0.40). These results suggest that stacked ML-4 provides the most accurate predictions for flexural strength. Stacked ML-1 and stacked ML-2 follow closely with R^2 values of 0.977 each. While their error metrics are slightly higher than those of stacked ML-4, they still offer reliable predictions for flexural strength. Stacked ML-3 and stacked ML-5 show lower performance, with higher MSE and RMSE values, indicating less accurate predictions. Stacked ML-3, in particular, has the highest RMSE (0.74) and MAE (0.45), making it the least optimal model for flexural strength prediction.

Noteworthy, for tensile strength, stacked ML-4 improved in tensile strength prediction, achieving the highest R^2 value of 0.983 and the lowest error metrics, including MSE (0.04), RMSE (0.20), and MAE (0.16). This suggests that stacked ML-4 is the most accurate model for tensile strength prediction. Stacked ML-5 and Stacked ML-3 also perform well, with R^2 values of 0.972 and 0.946, respectively, and reasonably low error metrics. These models provide good alternatives for tensile strength prediction. Stacked ML-1 and Stacked ML-2 exhibit lower performance with R^2 values of 0.939 and 0.915, respectively. Their higher error metrics indicate less accurate predictions, with stacked ML-2 having the highest RMSE (0.45) and MAE (0.33), making it less favorable for tensile strength prediction.

It is clear that the stacked ML-2 can be introduced for compressive strength and stacked ML-4 is the best model for flexural and tensile strengths of FR-PAC. It also presents the ability of those tree-based ML models of BR, ETR, and RF (i.e., stacked ML-2) and boosting-based ML models of LGBM, XGBoost, and GBM (i.e., stacked ML-4) to be in parallel processing on prediction of the mechanical properties. However, using the idea of optimization-based multi-target stacked ML model improved those performance of single-target stacked ML models, and this can increase the accuracy of prediction even in the limited number of datasets.

7 Graphical user interface

Introducing the best-stacked ML models and validating them by experimental tests in previous sections show that they have a superior capability to be used by researcher to reduce the cost of experimental tests and increase the accuracy and speed of finding the best mixture for PAC and FR-PAC. Therefore, the GUI was designed for

Optimization-Based Multi-Target Ensemble ML Model For Estimating Properties of PAC and FR-PAC

Developed by Farzin Kazemi

Input Parameters

Cement	<input type="text"/>	(kg/m ³)
Sand	<input type="text"/>	(kg/m ³)
Water	<input type="text"/>	(kg/m ³)
Water/Binder	<input type="text"/>	(%)
Sand/Binder	<input type="text"/>	(%)
Gravel	<input type="text"/>	(kg/m ³)
Fly Ash	<input type="text"/>	(kg/m ³)
Silica Fume	<input type="text"/>	(kg/m ³)
Slag (GGBS)	<input type="text"/>	(kg/m ³)
Metakaolin	<input type="text"/>	(kg/m ³)

Input Parameters

Limestone Powder	<input type="text"/>	(kg/m ³)
Superplasticizer	<input type="text"/>	(kg/m ³)
Expanding Admixture	<input type="text"/>	(kg/m ³)
Steel Fiber	<input type="text"/>	(%)
Fiber Length	<input type="text"/>	(mm)
Fiber Diameter	<input type="text"/>	(mm)
Fiber Aspect	<input type="text"/>	(%)
Fiber Tensile Strength	<input type="text"/>	(MPa)
Polypropylene Fiber	<input type="text"/>	(%)

Preplaced Aggregate Concrete

- Compressive Strength
- Tensile Strength
- Flexural Strength
- 7 Days (MPa)
- 28 Days (MPa)
- 90 Days (MPa)

Fiber-Reinforced Preplaced Aggregate Concrete

- Compressive Strength
- Tensile Strength
- Flexural Strength
- 7 Days (MPa)
- 28 Days (MPa)
- 90 Days (MPa)

Default Input Dataset Predict Save Cancel

Fig. 25 Proposed GUI using ensemble ML models for estimating mechanical properties, axial load-displacement, and stress-strain curves of CTFSTs

stacked ML models to predict mechanical strengths of experimental specimens in PAC and FR-PAC as a crucial tool for engineers and designers. This GUI presented in Fig. 25 enables users to input detailed material properties as they have the highest effect on the mechanical properties and see how they can affect the mechanical properties.

This ability can improve the accuracy of selecting the mixture ingredient of PAC and FR-PAC and reduce the cost of constructing experimental specimens as well as reducing the environmental effects of the debris of experiments. Once the data is entered in input parameters, users can use the ability of various pre-trained stacked ML models tailored for different strength predictions. It is also equipped with the ability of updating the datasets for future investigations and this can further improve its ability. Using these features, the GUI helps users quickly interpret results, select the most accurate inputs, and make informed decisions based on predictive insights. Additionally, the ability to export results supports comprehensive reporting and documentation. Overall, this GUI enhances the efficiency of the design process, ensuring reliable and precise strength predictions for PAC and FR-PAC specimens.

8 Future studies on PAC and FR-PAC

Future studies on PAC and FR-PAC should focus on several key areas to advance their application in structural members. Firstly, it is crucial to investigate the long-term durability of PAC and FR-PAC under varying environmental conditions. Studies should include accelerated aging tests to assess how these materials withstand factors such as moisture, temperature fluctuations, and chemical exposure over extended periods. Additionally, there is

a need for more comprehensive research on the optimal types and dosages of fibers used in FR-PAC. Although this research included many of those input features that affect the mechanical properties, the limited literature in this area may ignore other environmental features like temperature and curing condition.

Another area for future study involves the development of standardized guidelines for the design and application of PAC and FR-PAC. These guidelines should address the integration of these materials into structural design codes, ensuring that they are adequately represented in terms of load-bearing capacities, safety factors, and construction practices. The exploration of advanced modeling techniques, such as ensemble ML algorithms [65], active learning method [67] and finite element analysis, to predict the performance of PAC and FR-PAC in various structural configurations will be beneficial. Such models should be validated with extensive experimental data to ensure accuracy. Research should also focus on the sustainability aspects of PAC and FR-PAC. This includes investigating the environmental impact of production processes and the potential for using recycled materials or industrial byproducts as partial replacements in the mix. The economic feasibility of implementing PAC and FR-PAC on a larger scale should be analyzed, considering factors such as cost-effectiveness, ease of production, and integration into existing construction practices. Since the database of proposed GUI can be updated by a new dataset, this can be added for future generation of GUI and consider those effects into account.

9 Conclusions

This paper investigates PAC and FR-PAC as unique form of concrete that can be used in marine structures and heavyweight concrete members. These materials have got attention due to their enhanced mechanical properties, durability, and potential for high performance in challenging environments. Therefore, this research focused on introducing optimization-based multi-target stacked ML models for estimating mechanical properties of PAC and FR-PAC as novel estimation tool for designers. Moreover, experimental tests have been performed to prepare unseen dataset to validate the generality of those proposed stacked ML models. The study achieved the following results:

- The results of stacked ML models on the experimental dataset can confirm the superior accuracy of them and the procedure used for optimizing them on different type of datasets. It also presents the ability of those tree-based ML models of BR, ETR, and RF (i.e., stacked ML-2) and boosting-based ML models of LGBM, XGBoost, and GBM (i.e., stacked ML-4) to be in parallel processing on prediction of the mechanical properties of PAC and FR-PAC.
- For estimating the mechanical properties of PAC, stacked ML-4 had the highest R^2 value of 0.964, indicating the lowest MSE of 1.78 and RMSE of 1.34. However, stacked ML-1 had the lowest MARE of 0.072 and MSRE of 0.036, suggesting it provides the most accurate predictions relative to the actual values. As it is presented, stacked ML-1, stacked ML-3, stacked ML-4 and stacked ML-5 had the accuracy of predictions higher than 95.5% that shows their superior performance.
- To predict the mechanical properties of FR-PAC, stacked ML-2 has the highest R^2 value of 0.956, indicating the best fit to the data with the lowest MSE of 1.54, RMSE of 1.24, and MAE of 0.67. Stacked ML-1 and stacked ML-4 also perform well but fall behind stacked ML-2 in almost all metrics. The comparison on the erMAX (maximum relative error) show that all proposed stacked ML models had the lowest erMAX indicating the highest reliability in predicting the mechanical properties of FR-PAC.
- For flexural strength, stacked ML-4 achieved the highest R^2 value of 0.981, for tensile strength, stacked ML-4 and stacked ML-5 both models have the highest R^2 values of 0.982, indicating the best fit for flexural and tensile strengths. Therefore, stacked ML-4 is a highly reliable model, especially for predicting flexural and tensile strengths, while stacked ML-2 is superior in predicting compressive strength.
- Validating the proposed ML methods with experimental tests of PAC show that stacked ML-4 had the best-performing model for compressive strength with the highest R^2 value of 0.974, and for tensile strength, stacked

ML-1 and stacked ML-5 performed well, with R^2 values of 0.957 and 0.951, respectively. However, for tensile strength, stacked ML-5 showed the most accurate model with the highest R^2 value of 0.947 and the lowest MSE of 0.02 and RMSE of 0.15.

- Experimental tests of FR-PAC were used for compressive, flexural, and tensile strengths. Results show that stacked ML-2 achieves the highest performance for compressive strength prediction with an impressive R^2 value of 0.986, stacked ML-4 showed the best performance for prediction of flexural and tensile strengths of FR-PAC with the highest R^2 value of 0.980 and 0.983, respectively.
- For the beneficial of designers, the best stacked ML models were implemented on the GUI to predict compressive, flexural, and tensile strengths of experimental specimens in PAC and FR-PAC. This ability can improve the accuracy of selecting the mixture ingredient of PAC and FR-PAC and reduce the cost of constructing experimental specimens as well as reducing the environmental effects of those debris of experiments. The database of GUI can be updated in future for including more dataset and input features.

Acknowledgments The authors would like to thank Professor Robert Jankowski for his guidance and help in preparing this paper. This work was conducted during an outgoing mobility grant that was funded by the project "Gdańsk Tech Doctoral School closer to Europe" (project/contract number: BPI/STE/2023/1/00018/DEC/ 01; task internal number: 037162, acronym: "PG_go_West"), co-financed by the Polish National Agency for Academic Exchange (NAWA) under the Programme "STER - Internationalisation of Doctoral Schools". Numerical calculations were carried out at the Tri-City Academic Supercomputer and Network (*CI TASK*) in Gdańsk, Poland.

Author contributions MAS: Writing—original draft, Data curation, Conceptualization, Experiments, Resources, Validation. FK: Writing—original draft, Supervision, Conceptualization, Methodology, Formal analysis, Software, Resources, Validation. HSA: Writing—review and editing, Supervision. HFI: Writing—review and editing, Supervision.

Data availability All datasets are available on "Saleh M. A., Kazemi F., Abdelgader HS., Isleem H. F. Optimization-based multitarget stacked machine-learning model for estimating mechanical properties of conventional and fiber-reinforced pre-placed aggregate concrete, Mendeley Data, V1, 2025. <https://doi.org/10.17632/wt52w9g9p5.1>" (<https://data.mendeley.com/datasets/wt52w9g9p5/1>).

Declarations

Conflict of interest The authors declare that they have no conflict of interest.

Informed consent This paper has not been published elsewhere nor has it been submitted for publication elsewhere.

Open Access This article is licensed under a Creative Commons Attribution 4.0 International License, which permits use, sharing, adaptation, distribution and reproduction in any medium or format, as long as you give appropriate credit to the original author(s) and the source, provide a link to the Creative Commons licence, and indicate if changes were made. The images or other third party material in this article are included in the article's Creative Commons licence, unless indicated otherwise in a credit line to the material. If material is not included in the article's Creative Commons licence and your intended use is not permitted by statutory regulation or exceeds the permitted use, you will need to obtain permission directly from the copyright holder. To view a copy of this licence, visit <http://creativecommons.org/licenses/by/4.0/>.

References

1. ACI 304.1. Guide for the use of preplaced aggregate concrete for structural and mass concrete applications. 1997.
2. Najjar MF, Soliman AM, Nehdi ML. Two-stage concrete made with single, binary and ternary binders. *Mater Struct*. 2016;49(1–2):317–27.
3. Najjar MF, Soliman AM, Nehdi ML. Grouts incorporating supplementary cementitious materials for two-stage concrete. *J Mater Civil Eng*. 2017;29(6):04016298.
4. Mirza J, Mirza MS, Roy V, Saleh K. Basic rheological and mechanical properties of high-volume fly ash grouts. *Constr Build Mater*. 2002;16(6):353–63.
5. Malhotra VM. Fly ash, slag, silica fume, and rice husk ash in concrete: a review. *Concr Int*. 1993;15(4):23–8.

6. O'Malley J, Abdelgader HS. Investigation into viability of using two-stage (pre-placed aggregate) concrete in Irish setting. *Front Arch Civil Eng China*. 2010;4(1):127–32.
7. Abdelgader HS, Elgalhud AA. Effect of grout proportions on strength of two-stage concrete. *Struct Concr*. 2015;9(3):163–70.
8. Das KK, Lam SSE. Effect of coarse aggregate size and grouting process on properties of preplaced aggregate concrete. In: *World congress on civil, structural, and environmental engineering*, 2019
9. Abdelgader HS, Kurpińska M, Amran M. Effect of slag coal ash and foamed glass on the mechanical properties of two-stage concrete. *Mater Today Proc*. 2022;58:1091–7.
10. Morohashi N, Meyer C, Abdelgader H. Concrete with recycled aggregates- two-stage production method. *CPI Concr Plant Int*. 2013:34–41.
11. Nehdi ML, Najjar MF, Soliman AM, Azabi TM. Novel steel fibre-reinforced preplaced aggregate concrete with superior mechanical performance. *Cem Concr Compos*. 2017;82:242–51.
12. Murali G, Asrani NP, Ramkumar VR, Siva A, Haridharan MK. Impact resistance and strength reliability of novel two-stage fibre-reinforced concrete. *Arab J Sci Eng*. 2019;44(5):4477–90.
13. Abbas S, Soliman AM, Nehdi ML. Exploring mechanical and durability properties of ultra-high performance concrete incorporating various steel fiber lengths and dosages. *Constr Build Mater*. 2015;75:429–41.
14. Abirami T, Loganaganandan M, Murali G, Fediuk R, Sreekrishna RV, Vignesh T, Karthikeyan K. Experimental research on impact response of novel steel fibrous concretes under falling mass impact. *Constr Build Mater*. 2019;222:447–57.
15. Saleh MA, Su Z, Zhang J. Novel sustainable steel fiber reinforced preplaced aggregate concrete incorporating Portland limestone cement. *Sci Rep*. 2024;14(1):10937.
16. Özyüksel ÇA, Farzin K, Torkan S. Grey wolf optimizer integrated within boosting algorithm: application in mechanical properties prediction of ultra high-performance concrete including carbon nanotubes. *Appl Mater Today*. 2025;42:102601.
17. Feng DC, Wang Z, Wu G. Progressive collapse performance analysis of precast reinforced concrete structures. *Struct Des Tall Spec Build*. 2019;28(5):e1588.
18. Kazemi F, Aybike ÖÇ, Torkan S, Neda A, Robert J. RAGN-R: a multi-subject ensemble machine-learning method for estimating mechanical properties of advanced structural materials. *Comput Struct*. 2025;308:107657.
19. Chithra S, Kumar SS, Chinnaraju K, Alfin AF. A comparative study on the compressive strength prediction models for High Performance Concrete containing nano silica and copper slag using regression analysis and Artificial Neural Networks. *Constr Build Mater*. 2016;114:528–35.
20. Ayat H, Kellouche Y, Ghrici M, Boukhatem B. Compressive strength prediction of limestone filler concrete using artificial neural networks. *Adv Comput Des*. 2018;3(3):289–302.
21. Kumar A, Arora HC, Kapoor NR, Mohammed MA, Kumar K, Majumdar A, Thinnukool O. Compressive strength prediction of lightweight concrete: machine learning models. *Sustainability (Switzerland)*. 2022;14(4):2404.
22. Nguyen H, Vu T, Vo TP, Thai HT. Efficient machine learning models for prediction of concrete strengths. *Constr Build Mater*. 2021;266:120950.
23. Zhang J, Ma G, Huang Y, Sun J, Aslani F, Nener B. Modelling uniaxial compressive strength of lightweight self-compacting concrete using random forest regression. *Constr Build Mater*. 2019;210:713–9.
24. Coo M, Pheeraphan T. Effect of sand, fly ash, and coarse aggregate gradation on preplaced aggregate concrete studied through factorial design. *Constr Build Mater*. 2015;93:812–21.
25. Ahmadi-Nedushan B. An optimized instance based learning algorithm for estimation of compressive strength of concrete. *Eng Appl Artif Intell*. 2012;25(5):1073–81.
26. Erdal HI. Two-level and hybrid ensembles of decision trees for high performance concrete compressive strength prediction. *Eng Appl Artif Intell*. 2013;26(7):1689–97.
27. Dabiri H, Kioumars M, Kheyroddin A, Kandiri A, Sartipi F. Compressive strength of concrete with recycled aggregate: a machine learning-based evaluation. *Cleaner Mater*. 2022;3:100044.
28. Iqbal MF, Javed MF, Rauf M, Azim I, Ashraf M, Yang J, Liu QF. Sustainable utilization of foundry waste: forecasting mechanical properties of foundry sand based concrete using multi-expression programming. *Sci Total Environ*. 2021;780:146524.
29. Arabshahi A, Gharaei-Moghaddam N, Tavakkolizadeh M. Development of applicable design models for concrete columns confined with aramid fiber reinforced polymer using multi-expression programming. *Structures*. 2020;23:225–44.
30. Gandomi H, Faramarzi A, Rezaee PG, Asghari A, Talatahari S. New design equations for elastic modulus of concrete using multi expression programming. *J Civil Eng Manag*. 2015;21(6):761–74.
31. Kaplan G, Öz A, Bayrak B, Aydın AC. The effect of geopolymer slurries with clinker aggregates and marble waste powder on embodied energy and high-temperature resistance in prepacked concrete: ANFIS-based prediction model. *J Build Eng*. 2023;67:105987.
32. Moaf FO, Farzin K, Hakim SA, Marzena K. Machine learning-based prediction of preplaced aggregate concrete characteristics. *Eng Appl Artif Intell*. 2023;123:106387.
33. Qureshi HJ, et al. Prediction of compressive strength of two-stage (preplaced aggregate) concrete using gene expression programming and random forest. *Case Stud Construct Mater*. 2023;19:e02581.

34. Javed MF, Fawad M, Lodhi R, Najeh T, Gamil Y. Forecasting the strength of preplaced aggregate concrete using interpretable machine learning approaches. *Sci Rep.* 2024;14(1):8381.
35. Abdellatief M, Leong SW, Norashidah MD, Kim HM, Ali NA, Ahmed E-S. Evaluating enhanced predictive modeling of foam concrete compressive strength using artificial intelligence algorithms. *Mater Today Commun.* 2024;40:110022.
36. Abdellatief M, Youssef MH, Mohamed TE, Leong SW, Ren JC, Kim HM. Investigation of machine learning models in predicting compressive strength for ultra-high-performance geopolymer concrete: a comparative study. *Construct Build Mater.* 2024;436:1368.
37. ASTM C939. Standard test method for flow of grout for preplaced-aggregate concrete (flow cone method). *ASTM Int.* 2010; 04(c).
38. Saleh MA. et al. Innovative use of Portland limestone cement and date palm ash in sustainable preplaced aggregate concrete grouts. *Struct Concr.* 2025
39. ASTM C938-16. Standard practice for proportioning grout mixtures for preplaced-aggregate concrete. *ASTM Int.* 2016; I(c).
40. ASTM C943. Standard practice for making test cylinders and prisms for determining strength and density of preplaced-aggregate concrete in the laboratory. West Conshohocken, PA, USA, 2002.
41. ASTM C1609. Standard test method for flexural performance of fiber-reinforced concrete (using beam with third-point loading). West Conshohocken, PA, USA, 2007.
42. Abdelgader HS. How to design concrete produced by a two-stage concreting method. *Cem Concr Res.* 1999;29(3):331–7.
43. Abdelgader HS, Górski J. Stress-strain relations and modulus of elasticity of two-stage concrete. *J Mater Civil Eng.* 2003;15(4):329–34.
44. Coo M, Pheeraphan T. Effect of sand, fly ash and limestone powder on preplaced aggregate concrete mechanical properties and reinforced beam shear capacity. *Constr Build Mater.* 2016;120:581–92.
45. Abdelgader HS, et al. Mechanical properties of two-stage concrete modified by silica fume. *Mag Civil Eng.* 2019;89(5):26–38.
46. Chairunnisa N, Ruzhanah H, Daniel LS. The properties of preplaced aggregate concrete technology contain the industrial waste-material and the various shapes and sizes of coarse aggregate. *IOP Conf Ser Mater Sci Eng.* 2022;1212(1):012036.
47. Krishna Das K. Development of high-performance preplaced aggregate concrete. Hong Kong Polytechnic University, Hong Kong, 2022.
48. Murali G, Abid S, Vatin N. Experimental and analytical modeling of flexural impact strength of preplaced aggregate fibrous concrete beams. *Materials.* 2022;15(11):3857.
49. Murali G, Haridharan MK, Abid SR, Mohan C, Singh Khera G, Bandhavi C. Compressive strength and impact strength of preplaced aggregate fibre reinforced concrete. *Mater Today Proc.* 2023.
50. Murali G, Abid SR, Ranjan R, Khera GS, Ramesh G, Dixit S. Repeated impact behavior of preplaced aggregate concrete incorporating different fiber types. *Mater Today Proc.* 2023.
51. Mohan KSR, Diviyabharrathi KB, Murali G. Research on the development of high impact resistant preplaced aggregate fibrous concrete by the inclusion of coarse aggregates coated with asphalt. *Arab J Sci Eng.* 2022;47(4):4265–86.
52. Ponnambalam N, Thangavel S, Murali G, Vatin NI. Impact strength of preplaced aggregate concrete comprising glass fibre mesh and steel fibres: experiments and modeling. *Materials.* 2022;15(15):5259.
53. Prasad N, Murali G. Exploring the impact performance of functionally-graded preplaced aggregate concrete incorporating steel and polypropylene fibres. *J Build Eng.* 2021;35:102077.
54. Karthikeyan M, Verapathran M, Abid SR, Murali G. The combined effect of glass fiber mesh and steel fiber on two-layered preplaced aggregate concrete against drop weight impact. *Materials.* 2022;15(16):5648.
55. Ram Prasad K, Murali G, Kathirvel P, Haridharan MK, Karthikeyan K. Experimental study on functionally graded steel fibre reinforced preplaced aggregate concrete. *Int J Eng Technol (UAE)*, 2018; 7(3.12) Special Issue 12, 2018.
56. Jaishankar P, Murali G, Salaimanimagudam MP, Amran YHM, Fediuk R, Karthikeyan K. Study of topology optimized hammerhead pier beam made with novel preplaced aggregate fibrous concrete. *Period Polytech Civil Eng.* 2020;65(1):287–98.
57. Murali G, Abid SR, Al-Lami K, Vatin NI, Dixit S, Fediuk R. Pure and mixed-mode (I/III) fracture toughness of preplaced aggregate fibrous concrete and slurry infiltrated fibre concrete and hybrid combination comprising nano carbon tubes. *Constr Build Mater.* 2023;362:129696.
58. Swaminathan P, et al. Experimental and statistical investigation to evaluate impact strength variability and reliability of preplaced aggregate concrete containing crumpled rubber and fibres. *Materials.* 2022;15(15):5156.
59. Ramakrishnan K, et al. Standard and modified falling mass impact tests on preplaced aggregate fibrous concrete and slurry infiltrated fibrous concrete. *Constr Build Mater.* 2021;298:123857.
60. Nehdi ML, Najjar MF, Soliman AM, Azabi TM. Novel eco-efficient two-stage concrete incorporating high volume recycled content for sustainable pavement construction. *Constr Build Mater.* 2017;146:9–14.
61. Alyousef R. Sustainable use of waste polypropylene fibres to enhance the abrasion and skid resistance of two-stage concrete. *Sustainability (Switzerland).* 2021;13(9):5200.

62. Kazemi F, Torkan S, Doo-Yeol Y. Data-driven modeling of mechanical properties of fiber-reinforced concrete: a critical review. *Arch Comput Methods Eng.* 2024;31(4):2049–78.
63. Kazemi F, Neda A, Torkan S, Robert J, Doo-Yeol Y. Machine-learning methods for estimating performance of structural concrete members reinforced with fiber-reinforced polymers. *Arch Comput Methods Eng.* 2025;32:571–603.
64. Shafighfard T, Kazemi F, Asgarkhani N, Yoo D-Y. Machine-learning methods for estimating compressive strength of high-performance alkali-activated concrete. *Eng Appl Artif Intell.* 2024;136: 109053.
65. Kazemi F, Neda A, Robert J. Optimization-based stacked machine-learning method for seismic probability and risk assessment of reinforced concrete shear walls. *Exp Syst Appl.* 2024;255:124897.
66. Asgarkhani N, Kazemi F, Jankowski R. Machine learning-based prediction of residual drift and seismic risk assessment of steel moment-resisting frames considering soil-structure interaction. *Comput Struct.* 2023;289: 107181.
67. Kazemi F, Shafighfard T, Jankowski R, Yoo D-Y. Active learning on stacked machine learning techniques for predicting compressive strength of alkali-activated ultra-high-performance concrete. *Arch Civil Mech Eng.* 2024;25(1):24.

Publisher's Note Springer Nature remains neutral with regard to jurisdictional claims in published maps and institutional affiliations.

Authors and Affiliations

M. A. Saleh^{1,2} · F. Kazemi^{3,4}  · H. S. Abdelgader⁵ · H. F. Isleem⁶

✉ F. Kazemi
farzin.kazemi@pg.edu.pl

M. A. Saleh
majed.saleh@uoz.edu.ly; majed.ali@mtc.edu.om

H. S. Abdelgader
h.abdelgader@uot.edu.ly

H. F. Isleem
mps565@york.ac.uk

¹ Civil Engineering Department, College of Engineering, University of Zintan, Zintan, Libya

² Department of Civil Engineering and Quantity Surveying, Military Technological College, Muscat, Oman

³ Faculty of Civil and Environmental Engineering, Gdańsk University of Technology, ul. Narutowicza 11/12, 80-233 Gdansk, Poland

⁴ School of Civil Engineering, National Technical University of Athens, 9 Iroon Polytechniou Str, 15772 Zografou, Greece

⁵ Department of Civil Engineering, Faculty of Engineering, University of Tripoli, Tripoli, Libya

⁶ Department of Computer Science, University of York, YO 10 5DD York, United Kingdom